COMPTES RENDUS
DE L'ACADÉMIE DES SCIENCES

Tome 12
fascicule 8

octobre 2011
ISSN 1631-0705

PHYSIQUE

DOSSIER

Quantum states of ultracold neutrons /
États quantiques des neutrons ultra froids

Guest editors / Rédacteurs en chef invités :
Ignatios Antoniadis, Valery Nesvizhevsky

ACADÉMIE DES SCIENCES − PARIS

ELSEVIER

Ultra cold neutron quantum states / États quantiques des neutrons ultra froids

Short-range fundamental forces

Forces fondamentales à courte portée

I. Antoniadis [a], S. Baessler [b,c], M. Büchner [d], V.V. Fedorov [e], S. Hoedl [f], A. Lambrecht [i],
V.V. Nesvizhevsky [g,*], G. Pignol [h], K.V. Protasov [h], S. Reynaud [i], Yu. Sobolev [j]

[a] *CERN, Geneve, CH-1211, Switzerland*
[b] *University of Virginia, Charlottesville, VA-22904, USA*
[c] *Oak Ridge National Laboratory, Oak Ridge, TN-37831, USA*
[d] *LCAR, Univ. Paul Sabatier, 115 route de Narbonne, Toulouse, F-31077, France*
[e] *PNPI, Orlova Roscha, Gatchina, RU-188300, Russia*
[f] *CENPA, Univ. of Washington, Seattle, WA 98195-4290, USA*
[g] *ILL, 6 rue Jules Horowitz, Grenoble, F-38042, France*
[h] *LPSC/IN2P3-UJF-INPG, 53 rue des Martyrs, Grenoble, F-38026, France*
[i] *LKB, ENS/UPMC/CNRS, Campus Jussieu, Paris, F-75005, France*
[j] *Inst. for Physics, Johannes Gutenberg-Univ. Mainz, 7 Staudingerweg, Mainz, G-55128, Germany*

A R T I C L E   I N F O

A B S T R A C T

We consider theoretical motivations to search for extra short-range fundamental forces as well as experiments constraining their parameters. The forces could be of two types: 1) spin-independent forces; 2) spin-dependent axion-like forces. Different experimental techniques are sensitive in respective ranges of characteristic distances. The techniques include measurements of gravity at short distances, searches for extra interactions on top of the Casimir force, precision atomic and neutron experiments. We focus on neutron constraints, thus the range of characteristic distances considered here corresponds to the range accessible for neutron experiments.

© 2011 Académie des sciences. Published by Elsevier Masson SAS. All rights reserved.

R É S U M É

Nous considérons les motivations théoriques pour rechercher des forces fondamentales supplémentaires à courte portée ainsi que des expériences contraignant leurs paramètres. Les forces peuvent être de deux types : 1) les forces indépendantes du spin ; 2) les forces dépendant du spin, de type axion. Différentes techniques expérimentales sont sensibles dans des domaines différents de distances caractéristiques. Les expériences incluent des mesures de gravité à courte distance, la recherche d'interactions supplémentaires en plus de la force de Casimir, des expériences atomiques et neutroniques de précision. Comme nous mettons l'accent sur les contraintes neutroniques, la gamme de distances caractéristiques considérées ici correspond à la plage accessible pour les expériences avec les neutrons.

© 2011 Académie des sciences. Published by Elsevier Masson SAS. All rights reserved.

* Corresponding author.

E-mail address: nesvizhevsky@ill.eu (V.V. Nesvizhevsky).

1. Introduction

The existence of other fundamental interactions in nature, mediated by new bosons, has been extensively discussed, given their possibility in many extensions of the Standard Model of particle physics [1–7]. Theories with large extra spatial dimensions provide strong motivation to search for such forces. If a boson is allowed to travel in large extra compactified dimensions, with a strong coupling constant in the bulk, it behaves in our 4d world as a very weakly coupled new boson, the coupling being diluted in the extra dimensions. The light dark matter hypothesis also argues in favor of the existence of new short range interactions. New bosons, for example, are predicted by most of the grand unified theories embedding the Standard Model, with the coupling constant of ∼0.1. These strongly coupled bosons have to be heavier than ∼1 TeV if they were not to conflict with present observations; heavier bosons will be searched for at the Large Hadron Collider. Lighter bosons could mediate a finite range interaction between two fermions:

$$V(r) = Q_1 Q_2 \frac{g^2}{4\pi} \frac{\hbar c}{r} e^{-\frac{r}{\lambda}} \tag{1}$$

where $V(r)$ is the interaction potential, g is the coupling constant, Q_1 and Q_2 are the charges of the fermions under the new interaction, and the range of this Yukawa-like potential $\lambda = \hbar/Mc$ is inversely proportional to the boson mass M. We consider the interactions of neutrons with nuclei of atomic number A, thus the charge of the atom under the new interaction is equal $Q_1 = A$, and the neutron charge is equal to unity $Q_2 = 1$. The presence of light bosons would be shown by deviations from the gravitational inverse square law.

The characteristic range of extra interactions, as well as their strength, varies largely in various theories. Therefore a phenomenological approach is chosen: searches for extra Yukawa-type forces are pursued over a very broad range λ. Nevertheless, in many cases one could point out promising distances. In theories with two large extra spatial dimensions, the characteristic range is ∼10^{-5} m; in theories with three large extra dimensions it is ∼10^{-8} m. Other numbers of extra spatial dimensions are ruled out by experiments or correspond to too small effects to be observed with known methods. In all mentioned interesting cases the ranges are accessible for neutron experiments: 10^{-10}–10^{-5} m; the optimum condition is usually met if $\lambda \sim \lambda_n$, where λ_n is the neutron wavelength. Concerning the strength of extra interactions, one should compare the constraints resulting from precision neutron experiments with those using all alternative methods. Searches for short-range modifications of gravity are most sensitive at distances $> 10^{-5}$ m [8,9]. Searches for extra forces on top of the van der Waals/Casimir–Polder (vdW/CP) forces give the best constraints in the nanometer range λ: $10^{-7(8)}$–10^{-5} m [10,11]. Exotic atoms constrain the sub-picometer domain: $< 10^{-12}$ m [12]. Even shorter distances are probed in high-energy accelerator experiments. Neutron constraints are most sensitive in the intermediate range of λ: 10^{-12}–10^{-8} m. In the range of λ: $10^{-8(7)}$–10^{-5} m neutron experiments could provide complementary information as well, and higher sensitivity in limited cases.

An attractive feature of neutrons is the smallness of false effects due to their electric neutrality. On the other hand, neutron experiments are strongly limited by the available statistics; this drawback might be overcome with new low-energy neutron sources. The current constraints for spin-independent short-range interactions as well as perspectives for their improvement using neutron experiments are shown in Fig. 1. The range of distances in this figure covers the range of interest for neutron experiments plus that for the best alternative methods on its lower and upper boundaries. In this plot, we give the limits for g^2 as defined in Eq. (1), and for α in another parameterization of spin-independent short-range interactions, where α is normalized to the strength of gravity:

$$V(r) = \alpha G \frac{m_1 m_2}{r} e^{-\frac{r}{\lambda}} \tag{2}$$

Here m_1 and m_2 are masses of the fermions that interact. Neglecting the small difference between the neutron mass m_n and the proton mass m_p we can translate:

$$g^2 = \frac{4\pi G m_n^2}{\hbar c} \alpha \tag{3}$$

The neutron constraints are derived:

1) From studies of neutron gravitational quantum states [13–17], based on data published in Refs. [18–20] (line 5 in Fig. 1). This first experiment has proven the existence of the phenomenon itself. Much more precise measurements seem to be feasible concerning both eventual systematic effects and statistical sensitivity [21,22]. First improvements might be expected in near future in flow-through-type experiments [23–25]; thus the sensitivity of [24] to new short-range interactions is discussed in [26], and is shown as line 9 in Fig. 1. In a second step we aim at large increase in sensitivity profiting from long storage of UCN in gravitational quantum states in the closed trap in the GRANIT spectrometer (line 10 in Fig. 1);

2) From the data on neutron whispering gallery effect [27–29] (line 6 in Fig. 1). This very first measurement provided already the absolute accuracy of measuring energy differences of quantum states significantly better than 10^{-3}, however, proper analysis of potential systematic effects has not yet been done. We present therefore a conservative estimation for the short-range-forces constraints based on the given accuracy that could be guaranteed on the present stage of our
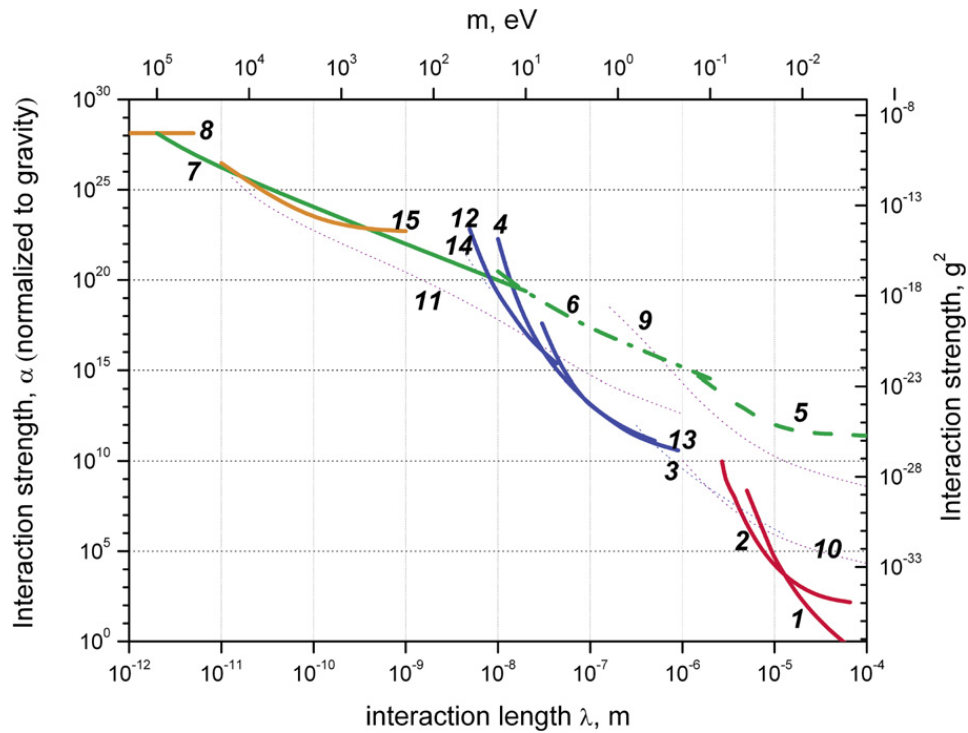
Fig. 1. The exclusion plot for new spin-independent interactions: limits on the interaction strength α, normalized to the gravitational interaction (on left), and the interaction strength g^2 (on right) are given as a function of the characteristic distance. The best currently constraints are shown in thick solid lines; preliminary results are indicated in thick dash-dotted lines; the best neutron constraints, but not the best currently available, are given in thick dashed lines; thin dotted lines in purple color correspond to projected sensitivity in various neutron experiments. Red color is reserved for measurements of gravity at short distances; blue-color constrains result from precision measurements of Casimir interactions; all constraints originated from neutron experiments are shown in green; constraint from measurements of exotic atoms is indicated in orange. Constraints "1" and "2" are obtained from measurements of short-range gravity in the torsion-balance [8] and the cantilever [9] experiment respectively. Constraints "4", "12" and "13" follow from measurements of extra forces on top of Casimir and van der Waals interactions in Refs. [11,35], in reanalysis presented in Ref. [10] of the experiment [36], and in Ref. [37] respectively. We do not show the limit "3" from Ref. [10], based on an experiment by Lamoreaux [38], as well as the limit "14" from Ref. [39], based on an experiment by Ederth [40], as solid constraints; Ref. [41] shows that correlations between fitted parameters deteriorate the sensitivity; furthermore a new systematical uncertainty was found [42] in the original experiment [38]. Constrain "5" follows from measurements of neutron gravitational quantum states [13]. Constrain "6" is derived from the data on neutron whispering gallery effect [30]. Constrain "7" follows from neutron scattering on nuclei [12]. Constrain "8" is obtained from analysis of precision measurements of exotic atoms [12]. Constrain "15" is obtained using searches for low-mass bosons from the Sun in a high-purity germanium detector [43]. Lines "9", "10", "11" correspond to our estimations of eventual improvements in neutron constraints following from measurements of gravitational quantum states in a flow-through mode, in storage mode using the GRANIT spectrometer, from quasi-elastic scattering of UCN at diluted noble gases and from neutron whispering gallery effect respectively.

Fig. 1. Figure d'exclusion pour une interaction supplémentaire indépendante du spin : l'intensité de l'interaction α normalisée par rapport à l'interaction gravitationnelle (axe de gauche) et l'intensité g^2 (à droite) sont reportées en fonction de la portée de l'interaction. Les meilleures contraintes actuelles sont indiquées par les lignes épaisses, les résultats préliminaires par des lignes épaisses discontinues, les meilleures contraintes neutroniques qui ne sont pas les meilleures disponibles sont indiquées par une ligne épaisse discontinue. Les lignes mauves en pointillé correspondent aux sensibilités attendues pour diverses expériences neutroniques. La couleur rouge est réservée pour les expériences de gravité à courte distance ; la couleur bleue concerne les expériences de mesure de la force de Casimir ; toutes les contraintes neutroniques sont indiquées en vert, les contraintes issues des atomes exotiques en orange. Les contraintes « 1 » et « 2 » sont obtenues en mesurant la gravité à courte distance avec un pendule [8] et une micropoutre [9] respectivement. Les contraintes « 4 », « 12 » et « 13 » proviennent des recherches d'une interaction supplémentaire s'ajoutant aux forces de Casimir et de Van der Waals dans [11,35], dans l'analyse de l'expérience [36] présentée dans [10], et dans [37] respectivement. Nous ne considérons pas comme contraintes solides la limite « 3 » de [10] basée sur l'expérience de Lamoreaux [38] ainsi que la limite « 14 » de [39] basée sur l'expérience de Ederth [40] ; en effet [41] la corrélation entre les paramètres ajustés détériore la sensibilité, de plus, une nouvelle erreur systématique a été découverte [42] dans l'expérience [38]. La contrainte « 5 » est issue de la mesure des niveaux quantiques gravitationnels du neutron [13]. La contrainte « 6 » est déduite de la mesure de l'effet galerie de chuchotement » [30]. La contrainte « 7 » est déduite des mesures de diffusion de neutrons par les noyaux [12]. La contrainte « 8 » est obtenue à partir de l'analyse des mesures de précision sur des atomes exotiques [12]. La contrainte « 15 » est obtenue en cherchant des bosons de faible masse produits par le Soleil en utilisant un détecteur Germanium de haute pureté. Les lignes « 9 », « 10 » et « 11 » correspondent à nos estimations des améliorations éventuelles des contraintes neutroniques en mesurant les niveaux quantiques gravitationnels en flux continu, en mode stockage avec le spectromètre GRANIT, par diffusion quasi-élastique des UCNs par un gas noble dilué et par l'effet « galerie de chuchotement », respectivement.

analysis, and will continue working on further improvements (line 11 in Fig. 1). The method to calculate the constraint is given in these proceedings [30];

3) From neutron scattering on nuclei [12]) (line 7 in Fig. 1). The idea of this method was proposed in Ref. [31]. Preliminary estimation of an even stronger constraint from neutron scattering on nuclei at shortest distances is available [32]; as the calculation procedure used there is based on possibly incomplete information, as stated by the author, on resonances in the nuclei used, as well as on complex multi-parametric mathematical analysis, without any study of global and local minima in the fit, it would be of interest to finalize the analysis and provide a reliable constraint. Concerning neutron scattering on nuclei, further improvements in sensitivity (line 11 in Fig. 1) are expected to follow from measurements
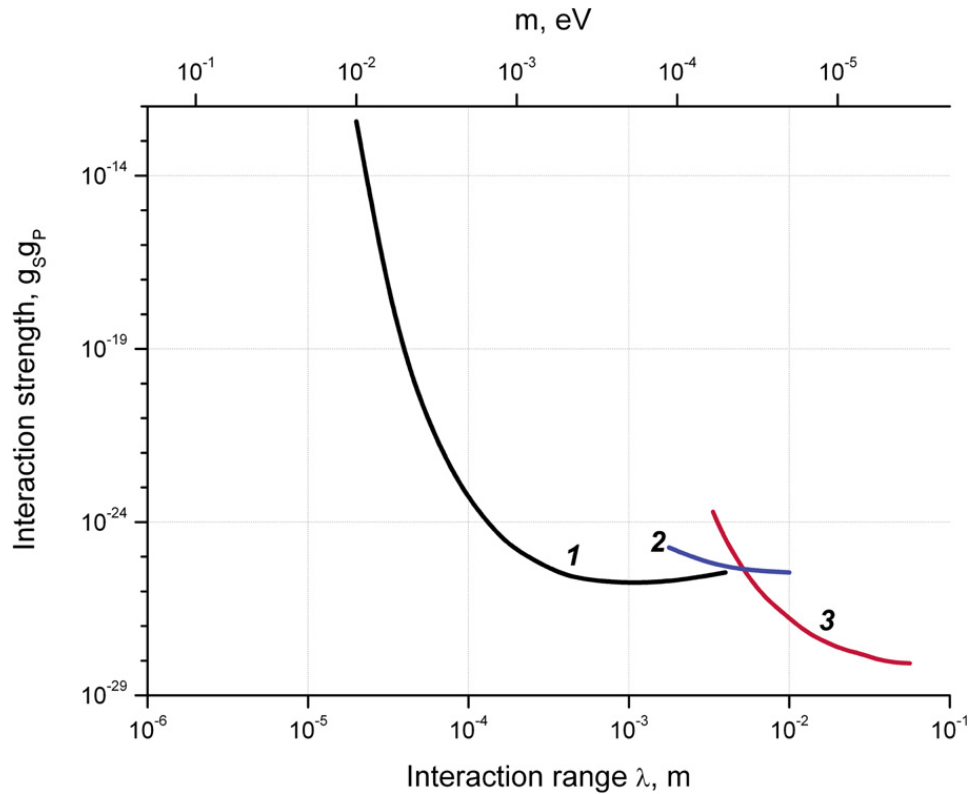
Fig. 2. Searches for short-range electron spin-dependent interactions. Each line is excluding the region to the top. The limit from [51] (1, black solid line) has been achieved with a (unpolarized) torsion pendulum made from silicon; and anomalous torque caused by a polarized electron source nearby has been searched for. Like in all these experiments, a big issue is the suppression of magnetic interactions. Successful elimination of magnetic anomalies can be tested in varying the distance between source and pendulum. The limit from [52] (2, blue solid line), the torque of an external circular mu-metal shield, polarized in a strong transverse magnetic field, on 3 unpolarized copper test masses coupled to a superconducting torsion pendulum in the center is measured. The usual magnetic field is strongly suppressed in the mu-metal shield, whereas an interaction as in Eq. (2) would cause a signal. The limit from [53] (3, red solid line) is derived from the response of a SQUID to the induced magnetization of a parametric salt by a (unpolarized) copper source mass rotating around the salt. Usual magnetic fields are shielded with a superconducting shield.

Fig. 2. Recherches d'interactions supplémentaires dépendant du spin de courte portée agissant sur les électrons. Chaque ligne exclue la région au-dessus. La limite [51] (1, ligne noire) est obtenue avec un pendule de torsion (non polarisé) de silicium, on recherche un couple anormal induit par une source d'électrons polarisés à proximité. Comme dans toutes ces expériences, le problème principal est de minimiser les interactions magnétiques. L'efficacité de l'élimination des anomalies magnétiques peut être vérifiée en faisant varier la distance entre la source et le pendule. La limite [52] (2, ligne bleue) est obtenue en mesurant le couple induit par un écran mu-métal externe polarisé dans un champ transverse intense sur 3 masses non polarisées de cuivre couplées à un pendule de torsion supraconducteur. Le champ magnétique usuel est fortement atténué dans l'écran en mu-métal tandis qu'une interaction du type eq. (2) induirait un signal. La limite [53] (3, ligne rouge) est obtenue à partir de la réponse d'un SQUID a la magnétisation induite d'un sel paramagnétique par une source (non polarisée) de cuivre tournant autour du sel. Les champs magnétiques usuels sont écrantés par un blindage supraconducteur.

of quasi-elastic scattering of UCN on atoms in diluted noble gases using gravitational spectrometers of total energy [30], and from measurements of asymmetry of scattering of slow neutrons on atoms in diluted noble gases [12]. A possibility of improving constraints using neutron-optical experiments is discussed in Ref. [33]. High-energy neutron–proton scattering on small angles was analyzed in view of getting constraints at even shorter distances than those presented in Fig. 1 in Ref. [34].

Many experiments look for spin-dependent short-range forces. Additional spin-dependent interaction could be caused by new, light, pseudo-scalar bosons such as the Axion. The Axion was originally proposed in Refs. [44–47] as a solution to the strong CP problem, caused by the smallness of the neutron electric dipole moment. The Axion would have profound consequences in cosmology and astrophysics [48], and the non-observation of these effects limits the Axion to have a mass in between approximately 10 μeV and 10 meV. The general form of the potential caused by the exchange of a pseudo-scalar, axion-like, boson between a polarized spin-1/2 particle and another unpolarized particle of the same kind is [49]:

$$V(r) = g_S^1 g_P^2 \frac{(\hbar c)^2}{8\pi m_2 c^2} (\sigma_2 \cdot \hat{r}) \left[\frac{1}{r\lambda} + \frac{1}{r^2} \right] \exp(-r/\lambda) \qquad (4)$$

Here, $g_S^1 g_P^2$ is the product of the relevant coupling coefficient between particle 1 (unpolarized) and 2 (polarized), and gives the strength of the potential. m_2 and σ_2 are the mass and the spin of the polarized particle, r is the distance between the particles, and $\lambda = \hbar/mc$ is the Yukawa range of the new interaction. The Yukawa range is used as a free parameter in the analysis, as the mass m of the new exchange boson is not known a priori.

Most experiments look for new forces between electrons. More recently, much progress was made in searches for new forces between nucleons. Comparisons between the coupling strengths for electrons and nucleons require a particular model of the new interaction; therefore it is not given here. We summarize present searches in the following exclusion plots. Fig. 2 shows the exclusion for new interactions between electrons (a chapter in the recent review [50] has been devoted to this); the distance scale λ on this plot is chosen to be equal to that in Fig. 3 in order to facilitate comparison. Fig. 3 shows the exclusion for new interactions between nucleons. The range for the λ values shown here is given by optimum sensitivity of neutron and polarized ^{3}He experiments.

This article is organized as follows: Theoretical motivations to short-range interactions are overviewed in Section 2. Casimir force studies are analyzed in Section 3. Measurements of atom–surface van der Waals interaction and test of non-Newtonian gravitational interaction by atom interferometry are presented in Section 4. GRANIT constraints for Standard Model extensions are mentioned in Section 5. Eventual constraints for spin-dependent short-range forces from the GRANIT experiment are derived in Section 6. A torsion pendulum searches for axion and exotic forces are overviewed in Section 7, in particular a new large improvement for constraints for such forces is presented. New experimental constraints
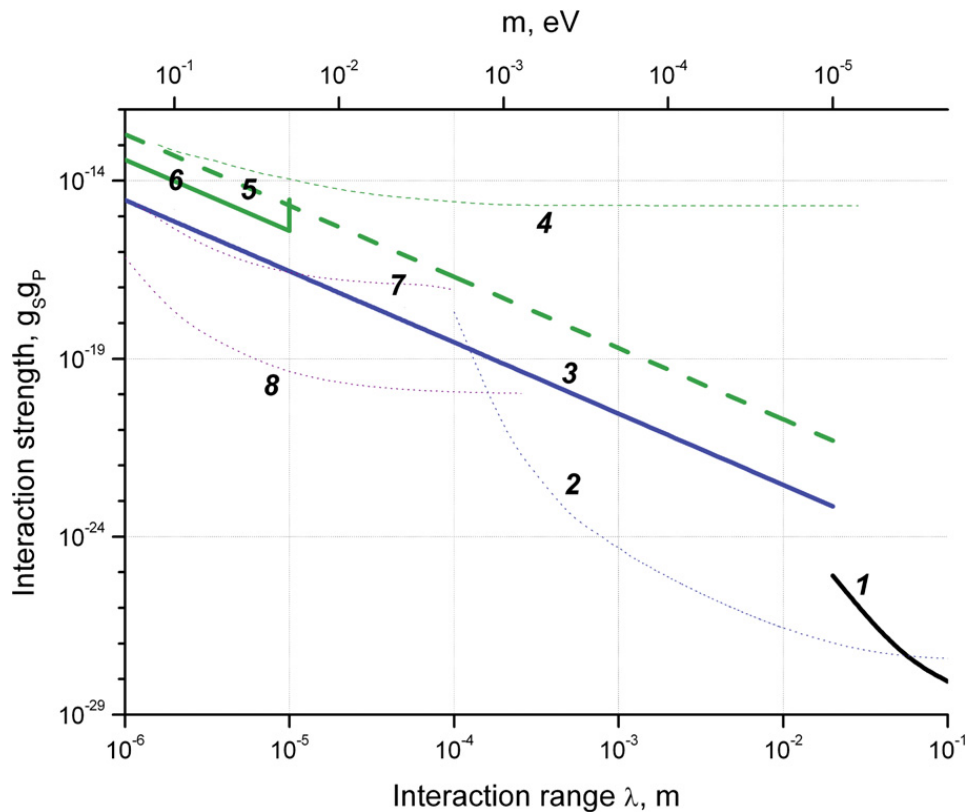

Fig. 3. Searches for short-range nucleon spin-dependent interactions. Each line is excluding the region to the top. The limit from [54] (1, black solid line) was achieved by comparing the precession frequencies of atomic magnetometers made from either ^{199}Hg or Cs atoms in presence of a 475 kg source mass made from lead. The sensitivity of the experiment with polarized ^{3}He, described in Section 9, is indicated in (2, thin dotted blue line). The limit from Ref. [55] (3, blue solid line) was derived from the spin relaxation rate in polarized ^{3}He cells; after subtraction of known causes of relaxation, the new interaction would constitute an extra relaxation channel. An even more constraining limit from experiments on storage of polarized ^{3}He has been proposed [56] but the validity of the method used is being questioned [57]. The limit in Ref. [58] (4, thin green dash-dotted line) was derived from the study of gravitationally bound states of ultra-cold neutrons; the publication [58] triggered much of the recent experimental activity on spin-dependent short-range nucleon–nucleon interaction presented in the present proceedings. The limit from Ref. [59] (5, thick green dashed line, proposed in [60]) was derived from comparison of the precession frequencies of ultra-cold neutrons in chambers in a vertical magnetic field, where the chamber bottom plate is made from a more dense material than top plate and vice versa. A force as in Eq. (2) changes the precession frequency with a sign which depends on the position of the denser plate. The limit from Ref. [61] (6, thick green solid line, criticized in Ref. [62]) was derived from the fact that a new short-range spin-dependent force would cause spin relaxation of ultra-cold neutrons in vicinity of a reflecting surface; limits on the depolarization probability were turned into limits on new forces of that kind. The transmission of polarized neutrons through a horizontal slit with an absorber at the top would look differently from the measurement if a sufficiently strong new interaction given by Eq. (2) would modify the wave functions of the gravitational bound states in dependence of their spin, as in a Stern–Gerlach experiment. We add projected sensitivities of different stages of the study of gravitationally bound quantum states: The constraint 7 is from a proposal to measure the neutron spin-dependent change of the transmission of UCNs through a horizontal slit made from an absorber and a mirror with GRANIT. This proposal was discussed in Ref. [164] (7, thin purple dotted line). The ultimate goal of GRANIT is to measure energy difference between quantum states of stored ultra-cold neutrons. Assuming an accuracy of 10^{-6}, which is achieved if the precision is just the natural line-width of the transition, and assuming this line width is limited only by the neutron beta decay lifetime, we get the second project limit (8, thin purple dotted line). In Ref. [63], a more optimistic scenario where a precision better than the size of the natural line width with the help of a Ramsey technique is discussed. An analogous method based on spin precession in a setup measuring neutron EDM and not requiring gravitational quantum states of neutrons is proposed in Ref. [64]. Finally, note that although most constraints presented on this figure are bound to the distance range corresponding approximately to the "axion window" there are no formal limitations for extending the range when considering axion-like particles; thus one should remember about experimental constraints at even shorter distances as those presented in Section 12.

Fig. 3. Recherches d'interactions supplémentaires dépendant du spin de courte portée agissant sur les nucléons. Chaque ligne exclue la région au-dessus. La limite [54] (1, ligne noire continue) est obtenue en comparant les fréquences de précession de magnétomètres atomiques utilisant des atomes de ^{199}Hg et Cs en présence d'une masse de plomb. La sensibilité des expériences avec ^{3}He polarisé (2, ligne bleue point-tilles) est décrite dans Section 9. La limite [55] (3, ligne solide bleue) a été obtenue par le taux de relaxation du spin dans les cellules de ^{3}He après correction des processus de relaxation connus, l'interaction supplémentaire constituant un canal de relaxation additionnel. Une meilleure limite a été proposée [56] à partir d'expériences de stockage de ^{3}He polarisé mais la validité de la méthode est remise en cause [57]. La limite [58] (4, ligne discontinue verte) est obtenue à partir de l'étude des niveaux quantiques du neutron dans le champ de pesanteur ; la publication [58] a enclenché un vaste programme expérimental pour sonder 'une interaction de courte portée nucléon–nucléon dépendant du spin qui fait l'objet de cet article. La limite [59], proposée dans [60] (5, ligne discontinue verte épaisse) est obtenue par comparaison de la fréquence de précession de neutrons ultrafroids dans un champ magnétique dans deux chambres de précession avec un matériau lourd en haut, léger en bas, et vice versa. Une interaction de type de l'eq. (2) modifierait la fréquence de précession avec un signe dépendant de la position du matériau dense. La limite [61] (6, ligne verte continue épaisse), critiquée dans [62], se base sur le fait que l'interaction supplémentaire provoquerait une relaxation du spin des neutrons ultrafroids au voisinage d'une surface réfléchissante ; les limites sur la probabilité de dépolarisation sont alors interprétées comme une limite sur une nouvelle interaction dépendant du spin. Si la nouvelle interaction donnée par l'eq. (2) est suffisamment intense, elle modifierait les fonctions d'onde des états quantiques du neutron dans le champ de pesanteur selon l'état de spin des neutrons et la courbe de transmission de neutrons non polarises à travers une fente horizontale avec un absorbeur au-dessus serait différente de celle observée, comme dans l'expérience de Stern et Gerlach. Nous considérons la sensibilité attendue pour les étapes futures de l'étude des niveaux quantiques : supposant une précision de 10^{-3} pour la mesure de la différence d'énergie entre l'état fondamental et le deuxième état excité dans l'expérience en flux continu de neutrons décrite dans cet ouvrage (Section 5 de la ref. [21]), un nouveau domaine de la figure d'exclusion dans le domaine micrométrique serait accessible (7, ligne mauve discontinue). Le but ultime de GRANIT est de mesurer les différences d'énergie des états quantiques en mode stockage de neutrons. Supposant la précision de 10^{-6} qui serait atteinte si la précision correspondait à la largeur naturelle de la transition pour des neutrons stockés pendant la durée de vie beta, nous obtenons la seconde limite attendue (8, ligne mauve discontinue). La ref. [63] présente un scenario plus optimiste ou une précision meilleure que la largeur naturelle pourrait être obtenue à l'aide de la technique de Ramsey. Une méthode analogue, basée sur la précession du spin dans un appareil mesurant le moment dipolaire électrique du neutron est proposée dans [64]. Finalement, il est à noter que la plupart des contraintes présentées sur cette figure sondent un domaine de distance correspondant à la « fenêtre de l'axion », mais il n'y a pas de raison fondamental empêchant de considérer des distances encore plus courtes, comme celles présentées en Section 12.

for spin-dependent short-range forces from storage of polarized ^{3}He are presented in Section 8; and those from ^{3}He/^{129}Xe clock comparison are given in Section 9. Constraints for short-range spin-independent short-range forces from neutron experiments are reproduced in Section 10. Constraints for spin-dependent interactions from could also be derived from neutron-EDM experiments using ultra-cold neutrons (Section 11), or from neutron-EDM experiments using propagation of cold neutrons in non-centrosymmetric crystals (Section 12); a largely improved new experimental constrain is presented in the later case.

2. Theoretical motivations to short-range interactions (Ignatios Antoniadis)

2.1. Strings and extra dimensions

In all physical theories, the number of dimensions is a free parameter fixed to three by observation, with one exception: string theory, which predicts the existence of six new spatial dimensions (seven in the case of M-theory). For a long time, string physicists thought that strings were extremely thin, having the smallest possible size of physics, associated to the Planck length $\sim 10^{-35}$ meters. However, the situation changed drastically over the recent years. It has been realized that the "hidden" dimensions of string theory may be much larger than what we thought in the past and they become within experimental reach in the near future, together with the strings themselves [1–4]. These ideas lead in particular to experimental tests of string theory that can be performed in particle colliders, such as LHC.

The main motivation came from considerations of the so-called mass hierarchy problem: why the gravitational force remains much weaker than the other fundamental forces (electromagnetic, nuclear strong and weak), at least up to present energies? In a quantum theory, the masses of elementary particles receive important quantum corrections, which are of the order of the higher energy scale present in the theory. Thus, in the presence of gravity, the Planck mass $M_P \sim 10^{19}$ GeV attracts all Standard Model particles to become 10^{16} times heavier than what they are. To avoid this catastrophe, one has to adjust the parameters of the theory up to 32 decimal places, resulting in a very ugly fine-tuning.

A possible solution is provided by the introduction of supersymmetry, which may be a new fundamental symmetry of matter. One of its main predictions is that every known elementary particle has a partner, called superparticle. Since none of these superparticles have ever been produced in accelerators, they should be heavier than the observed particles. Supersymmetry should therefore be broken. However, protection of the mass hierarchy requires that its breaking scale, i.e. the mass splitting between the masses of ordinary particles and their partners, cannot be larger than a few TeV. They can therefore be produced at LHC, which will test the idea of supersymmetry.

On the other hand, a new idea was proposed that solves the problem if the fundamental string length is fixed to 10^{-18}–10^{-19} m [4]. In this case, quantum corrections are controlled by the string scale, which is in the TeV region, and do not destabilize the masses of elementary particles. Moreover, it offers the remarkable possibility that string physics may be testable soon in particle colliders.

2.2. The string scale at the TeV

An attractive and calculable framework, allowing the dissociation of the string and Planck scales without contradicting observations, is provided by the so-called type I string theory. In this theory, gravity is described by closed strings
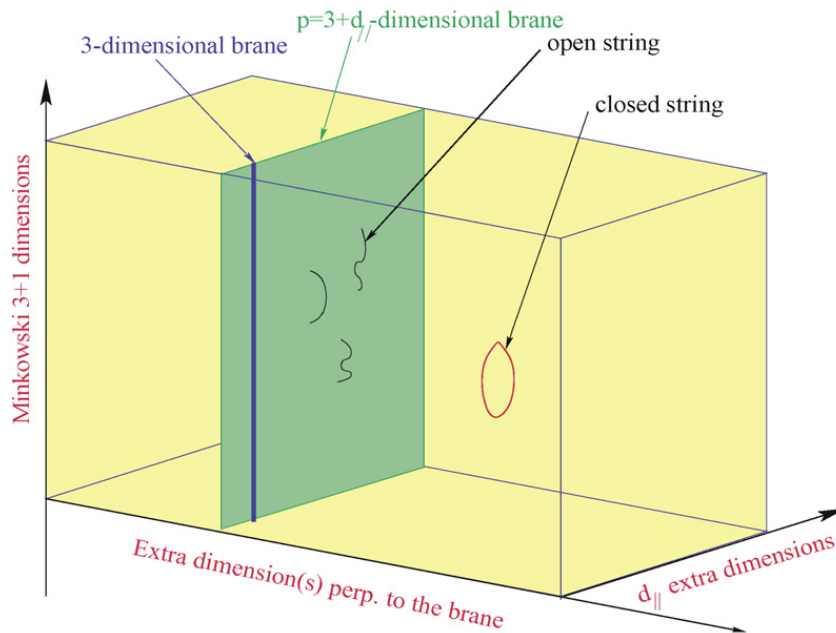
Fig. 4. In the type I string framework, our Universe contains, besides the three known spatial dimensions (denoted by a single blue line), some extra dimensions ($d_\| = p - 3$) parallel to our world p-brane (green plane) where endpoints of open strings are confined, as well as some transverse dimensions (yellow space) where only gravity described by closed strings can propagate.

Fig. 4. Dans le cadre de la théorie des cordes de type I, notre univers contient, en plus des trois dimensions spatiales connues (indiquées par la seule ligne bleue), des dimensions supplémentaires $d_\| = p - 3$ parallèles a notre p-brane (plan vert) où les extrémités des cordes ouvertes sont confinées, ainsi que des dimensions transverses (volume jaune) où seule la gravité, décrite par des cordes fermées, peut se propager.

which propagate in all nine dimensions of space, while matter and all other Standard Model interactions are described by open strings ending on the so-called D-branes. This leads to a braneworld description of our Universe, localized on a hypersurface, i.e. a membrane extended in p spatial dimensions, called p-brane (see Fig. 4). Closed strings propagate in all nine dimensions of string theory: in those extended along the p-brane, called parallel, as well as in the transverse ones. On the contrary, open strings are attached on the p-brane. Obviously, our p-brane world must have at least the three known dimensions of space. But it may contain more: the extra $d_\| = p - 3$ parallel dimensions must have a finite size, in order to be unobservable at present energies, and can be as large as $\mathrm{TeV}^{-1} \sim 10^{-18}$ m [1]. On the other hand, transverse dimensions interact with us only gravitationally and experimental bounds are much weaker: their size could reach 0.1 mm [8].

In the framework of type I string theory, the string scale M_s can be lowered in the TeV region at the expense of introducing large transverse dimensions of size much bigger than the string length. Actually, the string scale fixes the energy at which gravity becomes strongly coupled with a strength comparable to the other three interactions, realizing the unification of all fundamental forces at energies lower by a factor 10^{16} from what we thought in past. On the other hand, gravity appears to us very weak at macroscopic distances because its intensity is spread in the large extra dimensions [3]. The basic relation between the fundamental (string) scale and the observed gravitational strength is:

Total force = observed force x transverse volume

expressing the Gauss law for higher-dimensional gravity. In order to increase the gravitational force at the desired magnitude without contradicting present observations, one has to introduce at least two extra dimensions of size that can be as large as a fraction of a millimeter. At distances smaller than the size of extra dimensions, gravity should start deviate from Newton's law, which may be possible to explore in laboratory tabletop experiments [8,65,11,66,67,13,12] (see Fig. 9).

Type I string theory provides a realization of this idea in a coherent theoretical framework. Calculability of the theory implies that parallel dimensions should not be much bigger than the string length, while the size of transverse dimensions is fixed from the observed value of Newton's constant; it should thus vary from the Fermi scale (10^{-14} meters) to a fraction of a millimeter, depending on their number (varying from six to two, respectively). It is remarkable that this possibility is consistent with present observations and presents a viable and theoretically well motivated alternative to low energy supersymmetry, offering simultaneously a plethora of spectacular new phenomena that can be tested in laboratory experiments and be a surprise in LHC and other particle accelerators. The main experimental signal is gravitational radiation in the bulk from any physical process on the world-brane that gives rise to missing-energy. Explicit computation of these effects leads to the collider bounds given in Table 1.

Table 1

Collider bounds on the size of gravitational extra dimensions $R_\perp$ in mm.

Tableau 1

Limites sur la taille des dimensions supplémentaires gravitationnelles issues des collisionneurs.

Experiment	$n = 2$	$n = 4$	$n = 6$
LEP 2	5×10^{-1}	2×10^{-8}	7×10^{-11}
Tevatron	5×10^{-1}	10^{-8}	4×10^{-11}
LHC	4×10^{-3}	6×10^{-10}	3×10^{-12}

2.3. Short range forces

There are three categories of predictions in "table-top" experiments that measure gravity at short distances:

(i) Deviations from the Newton's law $1/r^2$ behavior to $1/r^{2+n}$, which can be observable for $n = 2$ large transverse dimensions of sub-millimeter size. This case is particularly attractive on theoretical grounds because of the logarithmic sensitivity of Standard Model couplings on the size of transverse space [68,69] that allows determining the hierarchy [70].

(ii) New scalar forces in the sub-millimeter range, related to the mechanism of supersymmetry breaking, and mediated by light scalar fields φ with masses: $m_\varphi \cong m_{susy}^2/M_P \cong 10^{-4}$–$10^{-6}$ eV, for a supersymmetry breaking scale $m_{susy} \cong 1$–10 TeV. They correspond to Compton wavelengths of 1 mm to 10 μm. m_{susy} can be either the compactification scale of parallel dimensions $1/R_\parallel$ if supersymmetry is broken by compactification [71,72] or the string scale if it is broken "maximally" on our world-brane [3,4]. A universal attractive scalar force is mediated by the radion modulus $\varphi \equiv M_P \ln R$, with R the radius of the longitudinal ($R_\parallel$) or transverse ($R_\perp$) dimension(s). In the former case, the above result follows from the behavior of the vacuum energy density $\Lambda \sim 1/R_\parallel^4$ for large $R_\parallel$ (up to logarithmic corrections). In the latter, supersymmetry is broken primarily on the brane, and thus its transmission to the bulk is gravitationally suppressed, leading to the same result. For $n = 2$, there may be an enhancement factor of the radion mass by $(\ln R_\perp)M_S \cong 30$, decreasing its wavelength by an order of magnitude [70]. The coupling of the radius modulus to matter relative to gravity can be easily computed and is given by:

$$\sqrt{\alpha_\varphi} = \frac{1}{M}\frac{\partial M}{\partial \varphi} \quad \text{with} \quad \alpha_\varphi = \begin{cases} \frac{\partial \ln \Lambda_{QCD}}{\partial \ln R} \cong \frac{1}{3} & \text{for } R_\parallel \\ \frac{2n}{n+2} = 1\text{–}1.5 & \text{for } R_\perp \end{cases}$$

where M denotes a generic physical mass. In the longitudinal case, the coupling arises dominantly through the radius dependence of the QCD gauge coupling [71,72], while in the case of transverse dimension, it can be deduced from the rescaling of the metric which changes the string to the Einstein frame and depends slightly on the bulk dimensionality ($\alpha_\varphi = 1$–1.5 for $n = 2$–6) [70]. Such a force can be tested in microgravity experiments and should be contrasted with the change of Newton's law due the presence of extra dimensions that is observable only for $n = 2$ [8,65,11,66,67,13,12]. The resulting bounds for the higher-dimensional gravity scale M_* from an analysis of the radion effects, are [73]: $M_* \succcurlyeq 6$ TeV (for $R_\perp$). In principle there can be other light moduli which couple with even larger strengths. For example the dilaton, whose vacuum expectation value determines the string coupling, if it does not acquire large mass from some dynamical mechanism, can lead to a force of strength 2000 times bigger than gravity [74].

(iii) Non-universal repulsive forces much stronger than gravity, mediated by possible abelian gauge fields in the bulk [3,75]. Such fields acquire tiny masses of order M_S^2/M_P, as in case (ii), due to brane localized anomalies [75]. Although their gauge coupling is infinitesimally small, $g_A \sim M_S/M_P \cong 10^{-16}$, it is still bigger that the gravitational coupling E/M_P for typical energies $E \sim 1$ GeV, and the strength of the new force would be 10^6–10^8 stronger than gravity.

In Fig. 5, we depict the actual information from previous, present and upcoming experiments [8,65,11,66,67,13,12]. The excluded regions lie above these solid lines. Measuring gravitational strength forces at short distances is challenging. The horizontal lines correspond to theoretical predictions, in particular for the graviton in the case $n = 2$ and for the radion in the transverse case. Finally, in Fig. 1 of the introduction of this chapter, recent improved bounds for new forces at very short distances are displayed by focusing on the left hand side of Fig. 5, near the origin [65,11,66,67,13,12].

2.4. Warped spaces

Braneworld models in curved space (warped metric) with non-compact extra dimensions may lead also to gravity modification at short distances. In particular in RS2, space–time is a slice of anti-de Sitter space (AdS) in $d = 5$ dimensions while our Universe forms a four-dimensional (4d) flat boundary [76]. The 4d Planck mass is given by: $M_P^2 = M_*^3/k$, with $k^2 = -\Lambda/24M_*^3$ in terms of the 5d cosmological constant Λ. Note that M_P is finite, despite the non-compact extra dimension in the 5d AdS space, because of the finite internal volume. As a result, gravity is kept localized on the brane, while the Newtonian potential gets corrections, $1/r + 1/k^2r^3$ which are identical with those arising in the compact case of two flat extra dimensions. Using the experimental limit $k^{-1} \preccurlyeq 0.1$ mm, one finds a bound for the 5d gravity scale $M_* \succcurlyeq 10^8$ GeV, corresponding to a brane tension $T \succcurlyeq 1$ TeV. Notice that this bound is not valid in the compact case of six extra dimensions, because their size is in the Fermi range and thus the $1/r^3$ deviations of Newton's law are cutoff at shorter distances.
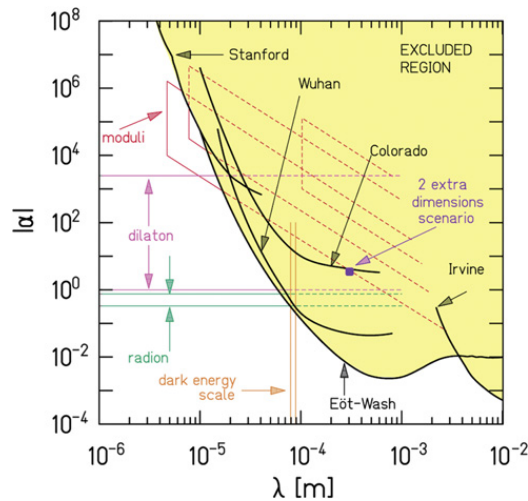
Fig. 5. Present limits on new short-range forces (yellow regions), as a function of their range λ and their strength relative to gravity α. The limits are compared to new forces mediated by the graviton in the case of two extra dimensions, and by the radion.

Fig. 5. Limites actuelles pour une nouvelle force de courte portée (région jaune), en fonction de la portée λ et de l'intensité relative à la gravite α. Les limites sont comparées aux nouvelles forces induites par le graviton dans le cas de deux dimensions supplémentaires, et par le radion.

3. The Casimir force studies (Serge Reynaud and Astrid Lambrecht)

The Casimir effect [77] is an observable effect of vacuum fluctuations visible on macroscopic objects, which deserves careful attention as a crucial prediction of quantum field theory [78–81].

It is also a fascinating interface between quantum electrodynamics and other important aspects of fundamental physics. It has connections with the puzzles of gravitational physics through the problem of vacuum energy [82] (and references therein) as well as with the principle of relativity of motion through the dynamical Casimir-like effects [83,84] (and references therein). It shows an extremely rich interplay with geometry [85,86] (more discussions below).

Casimir physics also plays an important role in the tests of gravity law at sub-millimeter ranges [87,88]. Strong constraints have been obtained in short range Cavendish-like experiments [8]: Should a hypothetical new force have a Yukawa-like form, its strength could not be larger than that of gravity if the range is larger than 56 μm. For scales of the order of the micrometer, similar tests are performed by comparing with theory the results of Casimir force measurements [89,66,90]. Other tests can be performed with atomic [90] or nuclear [12] force measurements (more discussions in other articles in this volume).

3.1. Comparison of the Casimir force measurements with theory

A new force would appear as a difference between the experimental measurement F_{ex} and the theoretical prediction F_{th} of the Casimir force. This implies that the accuracies of F_{ex} and F_{th} have to be assessed independently from each other.

Casimir calculated the force between a pair of perfectly smooth, flat and parallel plates in the limit of zero temperature and perfect reflection. He found universal expressions for the force $F_{Cas} = -\hbar c \pi^2 A / 240 L^4$ and energy $E_{Cas} = -\hbar c \pi^2 A / 720 L^3$ with L the inter-plate distance, A the area, c the speed of light and $\hbar$ the Planck constant. This universality comes from the saturation of the optical response of perfect mirrors which reflect 100% of the incoming fields. Clearly, this idealization does not correspond to any real mirror. The effect of imperfect reflection is large in most experiments, and a precise knowledge of its frequency dependence is essential for obtaining a reliable theoretical prediction for the Casimir force [91].

The most precise experiments are performed with metallic mirrors which are good reflectors at frequencies below the plasma frequency ω_P. Their optical response is described by a reduced dielectric function usually written at imaginary frequencies $\omega = i\xi$ as $\varepsilon(i\xi) = \hat{\varepsilon}(i\xi) + \sigma(i\xi)/\xi$. The function $\hat{\varepsilon}(i\xi)$ represents the contribution of inter-band transitions and is regular at the limit $\xi \to 0$; $\sigma(i\xi) = \omega_P^2/(\xi + \gamma)$ is the reduced conductivity (measured as a frequency) which describes the contribution of conduction electrons.

A simple description corresponds to the lossless limit $\gamma \to 0$ often called the plasma model. As $\gamma \ll \omega_P$ for a metal such as Gold, this model captures the main effect of imperfect reflection. However it cannot be considered as an accurate description since a much better fit of tabulated optical data is obtained with the Drude model which corresponds to a non-null value of the relaxation parameter γ. Furthermore, the Drude model meets the important property of ordinary metals which have a finite static conductivity $\sigma(0) = \omega_P^2/\gamma$, in contrast to the lossless limit which would correspond to an infinite value for $\sigma(0)$.

Another correction to the Casimir expressions is associated with the effect of thermal fluctuations [92,93] (and references therein). Even a small non-zero value of γ had a significant effect on the force evaluation at non-null temperature [94–96] (and references therein). After years of improvement of Casimir experiments, it now turns out that the most precise Casimir

experiments favor predictions obtained with $\gamma = 0$ rather with the expected $\gamma \neq 0$ (see Fig. 1 in Ref. [97]). The ratio between the predictions at $\gamma = 0$ and $\gamma \neq 0$ reaches a factor 2 at the limit of large temperatures or large distances. This large deviation is confirmed by microscopic descriptions of the Casimir interaction between two metallic bulks, which lead to predictions agreeing with the lousy Drude model rather than the lossless plasma model [98–100].

After this part of the overview was written, new experimental results have been published which favor the Drude model after subtraction of a large contribution of the patch effect: [101], see also the discussion in [102].

3.2. The role of geometry

The geometry of Casimir experiments might play an important role in this context. Precise experiments are indeed performed between a plane and a sphere whereas calculations are often devoted to the geometry of two parallel planes. The estimation of the force in the plane–sphere geometry involves the so-called "Proximity Force Approximation" (PFA) [103], which amounts to averaging over the distribution of local inter-plate distances the force calculated in the two-planes geometry, the latter being deduced from the Lifshitz formula [104,105]. This trivial treatment of geometry cannot reproduce the rich interconnection known to take place between the Casimir effect and geometry. In the plane–sphere geometry used for the experiments, the PFA can only be valid when the radius is much larger than the separation between the plates [106]. But even when this limit is met in experiments, the PFA does not tell one what is its accuracy for a given value of L/R or whether this accuracy depends on the material properties of the mirror. Answers to these questions can only be obtained by pushing the theory beyond the PFA, which has been done in the past few years (see references in [107–110]). In fact, it is only very recently that these calculations have been done with plane and spherical metallic plates coupled to electromagnetic vacuum [111], thus opening the way to a comparison with experimental studies of PFA in the plane–sphere geometry [112].

Another specific geometry of great interest is that of surfaces with periodic corrugations. As lateral translation symmetry is broken, the Casimir force contains a lateral component which is smaller than the normal one, but has nevertheless been measured in dedicated experiments [113,114]. Calculations beyond the PFA have first been performed with the simplifying assumptions of perfect reflection [115] or shallow corrugations [116–120]. The PFA was thus found to be accurate only at the limit of large corrugation wavelengths. Very recently, experiments have been able to probe the beyond-PFA regime [121,122] while it also became possible to calculate the forces between real mirrors with deep corrugations [123,124].

The best tool available for addressing these questions is the scattering approach which has been developed for years [125,126] and is now used by different groups using different notations [127–129]. It has also been used for analyzing other situations of interest, such as the torque appearing with non-aligned corrugations [130], or non-trivial effects of geometry which should be visible with atoms in a Bose–Einstein condensate used as a local probe of vacuum above a nano-grooved plate [131,132].

3.3. Discussion

At the end of this discussion, we have to face a lasting discrepancy between theory and experiment. This discrepancy may have various origins, in particular artefacts in the experiments or inaccuracies in the calculations. There may also exist yet unmastered differences between the situations studied in theory and the experimental realizations. Hence more work is needed to reach a reliable comparison of experiment and theory on the Casimir effect.

For example, the effect of temperature is also correlated with the plane–sphere geometry [133,134]. The first calculations accounting simultaneously for plane–sphere geometry, temperature and dissipation have been published very recently [135] and they show striking features. The factor of 2 between the long distance forces in Drude and plasma models is reduced to a factor below 3/2 in the plane–sphere geometry. Then, PFA underestimates the Casimir force within the Drude model at short distances, while it overestimates it at all distances for the perfect reflector and plasma model.

Experiments are performed with large spheres for which the parameter L/R is smaller than 0.01, and efforts are devoted to calculations pushed towards this regime [136]. If the results just reported were conserved for the experimental parameters $L/R < 0.01$, the actual values of the Casimir force calculated within plasma and Drude model could turn out to be closer than suggested by PFA, which would diminish the discrepancy between experimental results and predictions of the thermal Casimir force using the Drude model. Other possibilities are still open, and progress will hopefully result from ongoing work an experimental as well as experimental issues [137].

4. Measurements of atom–surface van der Waals interaction and test of non-Newtonian gravitational interaction by atom interferometry (Matthias Büchner, S. Lepoutre, H. Jelassi, G. Trénec, J. Vigué, V.P.A. Lonij, A.D. Cronin)

Atom interferometers have proven their capability to measure precisely interactions between atoms and their environment [138]. As with their optical analogues, it is possible to split coherently a matter wave, to perturb only one arm of the
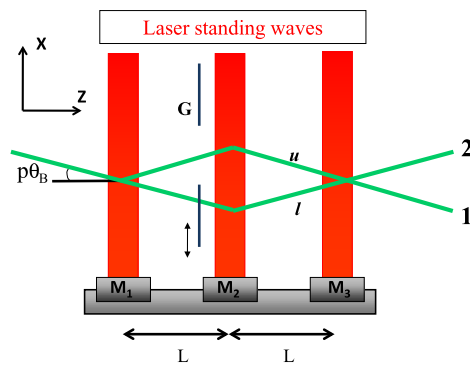
Fig. 6. Our atom interferometer. A supersonic lithium beam is strongly collimated by two thin slits. It then crosses three laser standing waves which play the role of beam-splitters and mirrors for the atom wave, thus forming a Mach–Zehnder atom interferometer. A nanograting *G* is introduced on one arm only and the phase shift of the interference fringes is measured as a function of the atom velocity.

Fig. 6. Un faisceau supersonique de lithium est fortement collimaté par deux fentes minces. Il traverse ensuite trois ondes stationnaires laser qui jouent le rôle de séparateur de faisceau et de miroirs pour l'onde d'atomes, formant ainsi un interféromètre atomique de Mach–Zehnder. Un nanoréseau *G* est introduit sur un seul bras et le déphasage des franges d'interférences est mesuré en fonction de la vitesse des atomes.

interferometer and to detect the perturbation on the interference signals. Several experiments of this type have been done, among which the measurement of atomic electric polarizability [139–141] and of the refraction index of gases for matter waves [142–144].

Atom–surface interaction is intensively studied in literature [145], in the van der Waals regime (i.e. for short atom–surface distance below ca. 100 nm) or in the Casimir–Polder regime (for longer ranges). This interaction has been studied by various atom optics experiments, by studying the diffraction of an atomic or molecular beam by a nanograting [146–148] or the reflection properties of a matter wave by an evanescent light field [149]. In 2005, J.D. Perreault and A.D. Cronin [150] used their sodium atom interferometer to measure the phase-shift of the atom wave transmitted by a nanograting in the zeroth-order beam and they showed that this phase-shift is due to the atom–surface interaction in the van der Waals regime. In the present paper, we describe a very similar experiment done with the Toulouse atom interferometer. We have been able to improve considerably the accuracy of the measurements for the following reasons: the Toulouse interferometer has a lower phase noise than the Arizona interferometer; the Arizona interferometer uses diffraction by nanogratings [150], which produces many diffracted beams and these beams complicate the analysis. The Toulouse interferometer, which uses Bragg diffraction on laser standing waves, produces essentially a Mach–Zehnder configuration with almost no stray beams and this simplifies considerably the analysis of the signals.

Our experimental arrangement, which is similar to the one of Ref. [150], is schematically represented in Fig. 6. Here is a brief description of our interferometer (for more details, see [151]). We use expansion of lithium seeded in a rare gas (pure or mixtures) to produce a supersonic atomic beam, with a velocity tunable over the 740–3400 m/s range by changing the carrier gas. This beam is strongly collimated by two thin slits, before crossing three laser standing waves which are produced by reflecting laser beams on mirrors M_1, M_2 and M_3. These laser standing waves play the role of beam-splitters and mirrors for the atom wave. The laser wavelength λ_L is chosen near the first resonance line of lithium at 671 nm, with a blue detuning, and we use the atom diffraction in the Bragg regime. The angle between the diffracted beams is $2p\Theta_B$ where p is the diffraction order and Θ_B is the Bragg angle given by $\Theta_B = \lambda_{dB}/\lambda_L$, where λ_{dB} is the de Broglie wavelength. For an atom velocity $v = 1000$ m/s, $\lambda_{dB} = 53$ pm and the Bragg angle is $\Theta_B = 80$ µrad. For first order diffraction and with the chosen value of the distance L between laser standing waves, $L = 0.6$ m the maximum arm separation is close to 100 µm (and to 200 µm for second order diffraction).

We introduce the Au/Pd coated silicon-nitride nanograting already used by J.D. Perreault and A.D. Cronin [150] in the interferometer arms. A 250 µm wide opening in the grating allows to study consecutively several configurations with 0, 1 or 2 interferometer arms going through the grating. By comparing the case where one arm goes through the grating and the other one through the opening to the case where both arms go through the opening, we can study the effect of the grating on the atom propagation. We have shown that only the zeroth-order diffraction beam contributes to the interference fringes (while the other diffraction order contribute to some stray intensity) and the effect of the nanograting is simply to multiply the amplitude of this beam by the zeroth-order diffraction amplitude. The phase of this diffraction amplitude does not vanish because of the existence of an atom–surface interaction and the observed fringe phase shift is equal to the phase Φ_0 of this amplitude.

This phase shift Φ_0 has been measured for six atom velocities and the results are plotted in Fig. 7b. The two data points with $v > 2000$ m/s were obtained with an interferometer using second order Bragg diffraction. This was needed to keep a sufficient arm separation but, in this case, the measurements are less accurate because of some stray beams due to residual first order Bragg diffraction. The experimental data points are very well fitted by a power law, $\Phi_0 \propto v^{-0.49}$ (the data point at 3350 m/s, which deviates from the general trend, was excluded from the fit).

Let us discuss briefly the calculation of this phase-shift (for more details, see our papers [90,152]). For an atom interaction with a homogeneous half-space, the atom–surface interaction in the van der Waals regime is given by $V_{vdW}(r) =$

$-C_3/r^3$, where r is the atom–surface distance and C_3 the van der Waals coefficient. The exact potential seen by an atom going through the nanograting would be very complex to evaluate and, as done by previous authors [146,150], we approximate the potential V_{vdW} for an atom in the channel between two grating bars by the potential caused by two infinite planes coincident with the two nearest grating walls and we then allow the potential to be 'on' only while the atom is between the grating bars. We take into account the exact nanograting geometry measured in a separate experiment [153]. Using the WKB approximation, it is possible to express the phase associated to each atom trajectory:

$$\phi(\xi) = \frac{1}{\hbar v} \int_0^{L_G} V_{vdW}(z, \xi; w, \alpha)\, \mathrm{d}z \tag{5}$$

$\phi(\xi)$ depends on the nanometer scale position of atom ξ within the nanograting. As the atom beam diameter is much bigger than the width w of the grating, one should consider all possible ξ positions. Using Fourier optics the complex diffraction amplitude A_0 for the 0th order diffraction can be written:

$$|A_0|e^{i\Phi_0} = \frac{1}{d} \int_{-w/2}^{w/2} \exp\big[i\phi(\xi)\big]\, \mathrm{d}\xi \tag{6}$$

We have tested the behavior of the van der Waals potential by using a more general potential of the form $V(r) = -C_p/r^p$ and we have varied p and C_p and plotted the chi-square χ^2 of the best fit. The minimum chi-square is obtained for $p = 2.9 \pm 0.1$, perfectly consistent with the $p = 3$ value of the non-retarded van der Waals interaction. For $p = 3$, we have found $C_3 = 3.25 \pm 0.2$ meV/nm^3, in good agreement with a theoretical evaluation of this coefficient. We have also explained the origin of the peculiar velocity dependence of the phase shift $\Phi_0 \propto v^{-0.49}$. An obvious $1/v$ factor appears in Eq. (5) but the integral of Eq. (6) is also velocity-dependent: this integral is similar to the Cornu-type integrals appearing in Fresnel diffraction theory and the phase shift is dominated by a range of atom–surface distance which also depends of the velocity. To give an example, for $v = 750$ m/s, the region around $\xi \approx 9$ nm contributes the most, while for $v = 3500$ m/s, this region is closer to the surface, around $\xi \approx 5$ nm. Our analysis can be extended to give constraints for a hypothetical non-Newtonian gravitational interaction. This is usually done by adding a Yukawa term to the Newton gravitational potential between two masses m_1 and m_2:

$$V_{grav} = -G\frac{m_1 m_2}{r}\big[1 + \alpha \exp(-r/\lambda)\big] \tag{7}$$

G is the gravitational constant, while λ and α are the range and the proportionality constants of the Yukawa term respectively. The normal gravitational interaction is too weak to be detected and we consider only the Yukawa term. The interaction between an atom and a nanograting bar of thickness e takes the following form:

$$V_{grav} = -2\pi G m_{Li} \rho \alpha \lambda^2 \big[\exp(-\xi/\lambda) - \exp\big(-(\xi + e)/\lambda\big)\big] \tag{8}$$

m_{Li} is the lithium atom mass, ρ is the nanograting density [90,152]. We substituted the vdW interaction in the integral of Eq. (5) by a modified potential, which is the sum of the vdW term and the non-Newtonian gravitational term (Eq. (8)). We have considered three values of the range λ ($\lambda = 1, 2, 10$ nm) and we have calculated the phase shift induced by this modified potential as a function of C_3, α and the velocity v.

For a small set of positive α values, we have plotted the chi-square value χ^2 as a function of the value of the C_3 coefficient. Fig. 7 shows these plots for $\lambda = 2$ nm and three different α values: for $\alpha = 10^{25}$, the non-Newtonian gravitational interaction is nearly negligible and the best fit is obtained for $C_3 = 3.23$ meV/nm^3 with $\chi^2 = 3.1$; for $\alpha = 10^{26}$, the best fit is obtained with $C_3 = 3.12$ meV/nm^3 and this moderate change of C_3 is perfectly acceptable, as C_3 is not very well known, but the larger chi-square value $\chi^2 = 4.2$, proves that the fit is less good; for $\alpha = 10^{27}$, we find a too low C_3 value, $C_3 = 2.55$ meV/nm^3 and a very large chi-square value $\chi^2 = 69.0$. We deduce from this analysis that for $\lambda = 2$ nm, $\alpha < 10^{26}$ and a similar bound is found if we consider negative α values.

Finally we can give the following constraints on λ, α: for $\lambda = 1$ nm, $|\alpha| < 10^{28}$; $\lambda = 2$ nm, $|\alpha| < 10^{26}$; for $\lambda = 10$ nm, $|\alpha| < 10^{23}$. Fig. 8 compares the present bounds to those available in the literature. Our results give similar bounds to those obtained by previous experiments ("vdW" [154,155], "Ederth" [40,39]) made with macroscopic samples of matter but our bounds are considerably less good than those obtained by neutron optics and interferometry experiments [156,12,157]. This is easy to understand: the van der Waals interaction of neutron is negligible because its electric polarizability (near 10^{-48} m^3 [157]) is many orders of magnitude weaker than the one of atoms (for example 2.43×10^{-29} m^3 for ^{7}Li [140]). In practice, in all the experiments only with ordinary matters, the upper bound on a non-Newtonian gravitational interaction will be a small fraction of the van der Waals interaction, this fraction decreasing with the error bars on the measurements.

We want to point out that, because of its small mass and large electric polarizability, lithium is not the best choice among the atoms if one wants to detect a non-Newtonian gravitational interaction. We have used it because we have a very efficient atom interferometer with excellent phase sensitivity and an arm separation sufficient for the present experiment. To improve the sensitivity to a non-Newtonian gravitational interaction, one should work with an atom with a larger mass and a smaller electric polarizability. A natural choice would be the heaviest non-radioactive rare gas, xenon: its mass to
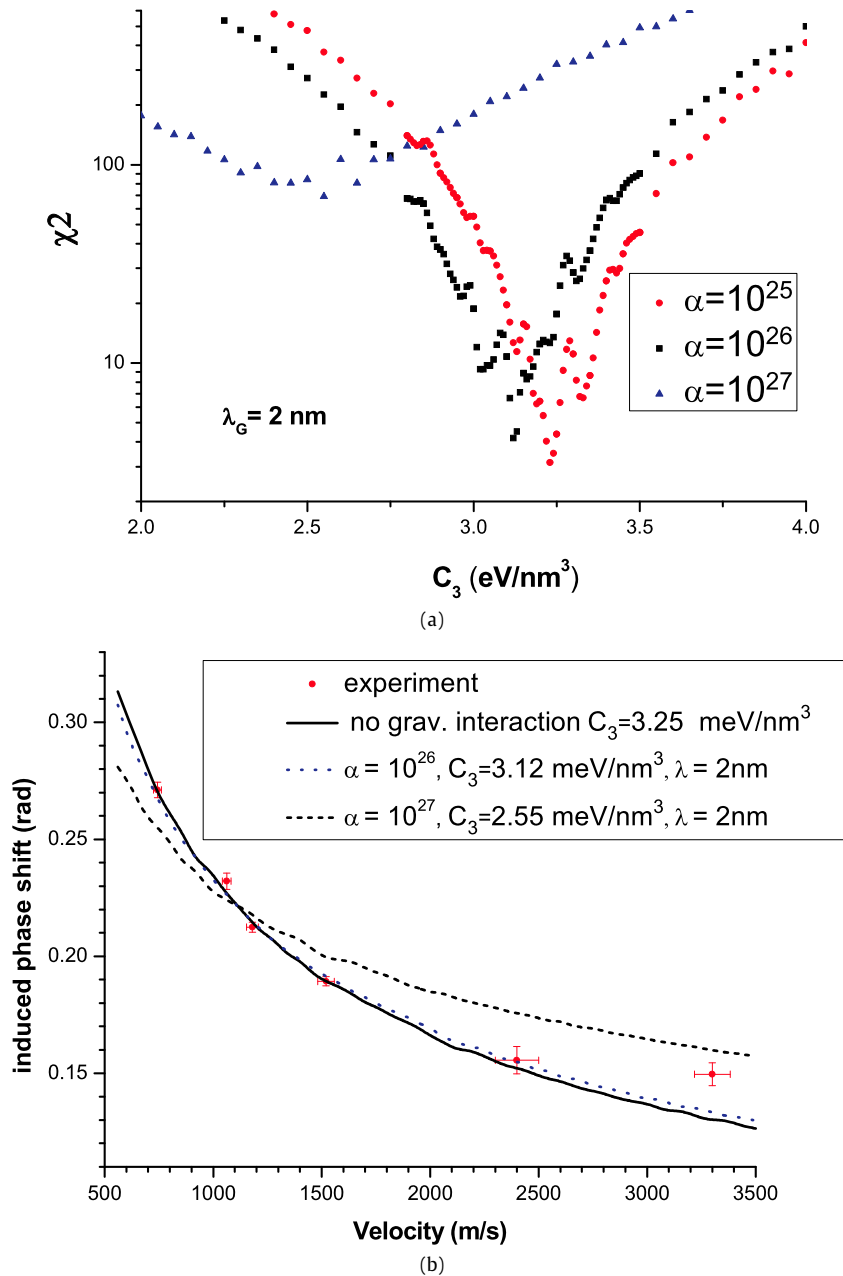
(a)

(b)

Fig. 7. a) χ^2 as a function of C_3 for three different α values ($\lambda = 2$ nm). b) Velocity dispersion of the induced phase shift for $\lambda = 2$ nm: we have plotted the calculated phase shift for $\alpha = 0$ (black full line), for $\alpha = 10^{26}$ (black dotted line) and $\alpha = 10^{27}$ (green dashed line), with in each case the C_3 value which minimizes χ^2.

Fig. 7. a) χ^2 en fonction de C_3 pour différentes valeurs de α ($\lambda = 2$ nm). b) Dispersion des vitesses du déphasage induit pour $\lambda = 2$ nm : nous avons reporté le déphasage calculé pour $\alpha = 0$ (ligne pleine noire), pour $\alpha = 10^{26}$ (ligne noire discontinue) et $\alpha = 10^{27}$ (ligne verte discontinue), avec dans chaque cas la valeur de C_3 qui minimise χ^2.

polarizability ratio is 33×10^{30} amu/m^3 [158], more than two orders of magnitudes larger than for ^{7}Li for which this ratio is 0.3×10^{30} amu/m^3. However, the only way of diffracting xenon atom is to use nanogratings and the readily available gratings, with a 100 nm period, will provide rather small diffraction angles (e.g. 60 µrad for a velocity $v = 500$ m/s) and this small angle will limit the interferometer arm separation.

Here, we have described a precision measurement of the van der Waals interaction between lithium and a nanograting, based on atom interferometry. The velocity dispersion of the observed phase shift proves that the atom–surface interaction is well described by the non-retarded van der Waals regime and we have measured the C_3 coefficient of this interaction with a 10% error bar. We have also tested the sensitivity of our experiment to detect a non-Newtonian gravitational interaction and, for a range λ between 1 and 10 nm, we have achieved a sensitivity comparable to those obtained by macroscopic experiments with ordinary matter. However, the sensitivity already achieved by neutron experiments for ranges in the nanometer region is considerably better than our own and even of what can be reached in a near future.
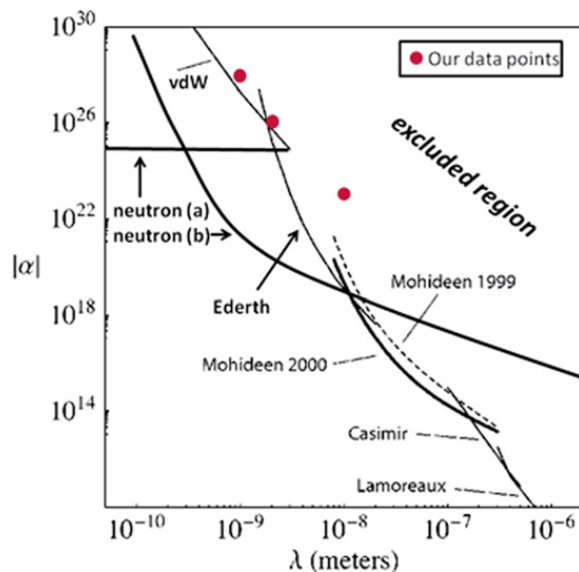
Fig. 8. Bounds for λ and α (figure taken from [157]). Our results give similar bounds to those obtained by previous experiments ("vdW" [154,155], "Ederth" [40,39]) made with macroscopic samples of matter. Neutron based experiments ("neutron (a), (b)") provide more restrictive bounds in the nanometer range of λ.

Fig. 8. Limites pour λ et α (figure provenant de [157]). Notre résultat donne des limites comparables à celles obtenues dans des expériences précédentes («vdW» [154,155], «Ederth» [40,39]) utilisant des échantillons macroscopiques de matière. Les expériences neutroniques («neutron (a), (b)») fournissent des limites encore plus restrictives dans le domaine nanométrique pour λ.

5. GRANIT constraints for Standard Model extensions (Orfeu Bertolami)

A particular class of extensions of the Standard Model of particle physics is related to non-commutative quantum mechanics [159–163].

6. Constraints for spin-dependent short-range forces from GRANIT (Stefan Baessler)

Constraints on spin-dependent short-range forces from the study of gravitationally bound states have been already discussed in other publications: The existing limit on spin-dependent short-range forces [58] was extracted from a previous measurement of the (unpolarized) neutron transmission through a slit made from a bottom mirror and a rough absorber [20]. The improvement that could be gained in a new measurement in the GRANIT spectrometer, in which one would use polarized neutrons for a similar measurement, is discussed in [164].

A measurement of energy differences between different neutron quantum states with GRANIT would allow setting up a superior limit. These measurements can be done with UCN stored in gravitationally bound quantum states. In order to show the sensitivity to new interactions, we assume that it is possible to achieve a precision in the energy differences between low-lying states $n \leftrightarrow l$ in the order of the natural line width, that is $\frac{\Delta E_{n\leftrightarrow l}}{E_{n\leftrightarrow l}}$ (see Section 9 in Ref. [21] for a more thorough discussion). The limit shown as curve 10 in Fig. 1 is computed by setting the energy shift due to a new short range interaction (as calculated in the first order perturbation theory) equal to $10^{-6} \cdot E_{n\leftrightarrow l}$. It is assumed that the bottom mirror is coated with tungsten or gold to increase the sensitivity. If the range of the new interaction λ is between 1 μm and 1 mm, the most sensitive transition is just the one between ground state and first exited state.

The sensitivity of the flow-through setup described in Section 5 in Ref. [21] to new short-range interactions is shown as curve 9 in Fig. 1. The curve is derived in [26]. Here, first order perturbation theory cannot be used to calculate the energy shift. The measurement of transition frequencies between energy levels of neutron quantum states in the gravitational field is sensitive to new spin-dependent short-range interactions too. The observable is then the possible change of the transition frequency with the direction of the neutron spin, as opposed to the value of the transition frequency used previously. The sensitivity is shown as curves 7, 8 in Fig. 3. For that limit, we assume a measurement precision of $10^{-6} \cdot E_{n\leftrightarrow l}$ but we don't assume a mirror coating. Again, for the relevant length ranges of the new interaction, the transition $1 \leftrightarrow 2$ is the most sensitive one.

7. A torsion pendulum based searches for axions and exotic forces (Seth Hoedl, E.G. Adelberger, B.R. Heckel)

Since the time of Cavendish, torsion pendulum based experiments have tested the fundamental forces of nature. Modern torsion pendulums achieve unprecedented sensitivity and impose some of the strongest constraints on extensions to the
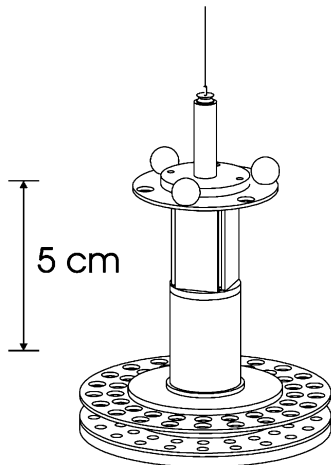
Fig. 9. A scale drawing of the ISL pendulum.
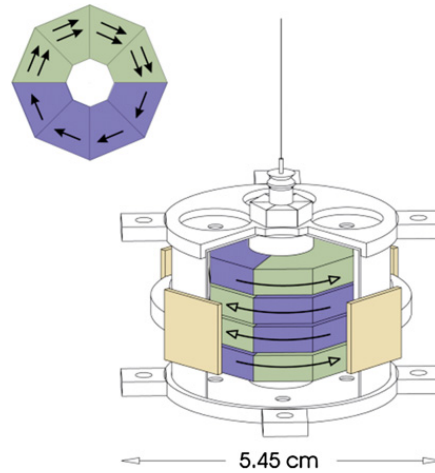
Fig. 9. Dessin à l'échelle du pendule ISL.

Fig. 10. A drawing of the spin pendulum. The blue material is SmCo$_5$. The green material is AlNiCo.

Fig. 10. Dessin du pendule de spin. Le matériau bleu est SmCo$_5$. Le matériau vert est AlNiCo.

Standard Model. The Eöt–Wash torsion balances operate with a very simple principle: an oscillating force or acceleration acting on a torsion pendulum generates an oscillating twist that can be observed by an autocollimator. The room temperature thermal noise of most of our experiments corresponds to an angular noise of approximately 1 nrad/$\sqrt{\text{day}}$. By observing the motion of almost a mole of atoms with such sensitivity, we impose interesting constraints on gravity-scale particle physics. A thorough review of the Eöt–Wash torsion pendulums and their theoretical motivations has recently been published [50]. Here we briefly summarize the results from three torsion pendulums that look for short-range deviations from Newton's Law of Gravitation [8], violations of Lorentz symmetry [165] and exotic forces mediated by axions or axion-like particles [51].

Precision measurements of the inverse square law (ISL) test a number of theoretical predictions. For example, the fat graviton scenario [166] and models with extra time dimensions [167] would weaken gravity at short distance scales, while the extra space dimensions of M-theory would strengthen gravity at scales smaller than the size of the largest compactified dimension [3]. The exchange of massive scalar or vector particles would also modify the ISL at short distances [168].

In our most recent ISL test [8], the torsion pendulum was suspended above a rotating attractor that consisted of two disks (see Fig. 9). 42 holes were machined in a 21-fold rotationally symmetric pattern into a molybdenum disk on the pendulum, called the detector, and into each disk of the attractor. The gravitational interaction between the missing mass in the detector and the attractor generated a torque that oscillated 21 times for each complete rotation of the attractor. The holes in the upper attractor disk were rotated by $\pi/21$ rad with respect to the holes in the lower attractor disk, so that when the bottom surface of the detector was 100 μm away from the top surface of the attractor, the Newtonian torque generated by each attractor disk canceled each other.

We parameterize deviations from the ISL by looking for a potential of the form:

$$V(r) = -G \frac{m_1 m_2}{r} \left(1 + \alpha \cdot e^{-r/\lambda} \right) \tag{9}$$

where λ and α are the range and strength of a Yukawa force respectively. Fig. 5 shows our most recent 2-σ limits. Our bounds imply that the maximum size of any extra dimension must be less than 44 μm. The ISL tests also impose many interesting constraints on scalar or vector particles [168]. For example, a coupling between a massive scalar and two photons will induce a modification to the ISL at short distances [169]. For a scalar mass of 1 meV/c^2, our results constrain the coupling strength $g_{\varphi\gamma\gamma} \leqslant 1.6 \times 10^{-17}$ GeV^{-1}. Note that this constraint is 10^{11} times smaller than the coupling that was claimed to explain the dichroism and birefringence of the vacuum initially observed by the PVLAS Collaboration [170,171].

We have also employed a torsion pendulum to look for interactions that couple to intrinsic spin [165]. In this apparatus, the torsion pendulum consisted of four octagonal "pucks" (see Fig. 10). One half of each puck was made of AlNiCo; the other half was made of SmCo$_5$. The magnetic field of AlNiCo is created almost entirely by electron spin; approximately half of the field of SmCo$_5$ is created by electron spin, and the balance is created by the orbital moment of the electrons. The magnetic field was contained in each puck, minimizing leaking magnetic fields; yet, each puck had a net spin moment of $\sim 10^{23}$ polarized electrons. The four pucks were arranged to minimize coupling to gravity gradients and to cancel a composition dipole that would make the pendulum sensitive to a violation of the equivalence principle. In this experiment, the torsion balance itself, including the optical read-out, rotated in the laboratory frame. By looking for a coupling of the pendulum's intrinsic spin to a preferred frame, we placed an upper bound of 10^{-22} eV on the energy required to flip an electron spin about an arbitrary direction fixed in inertial space. A preferred-frame arises not only in the context of Lorentz violation, but also in non-commutative space–time geometries predicted in some D-brane theories [172,173].
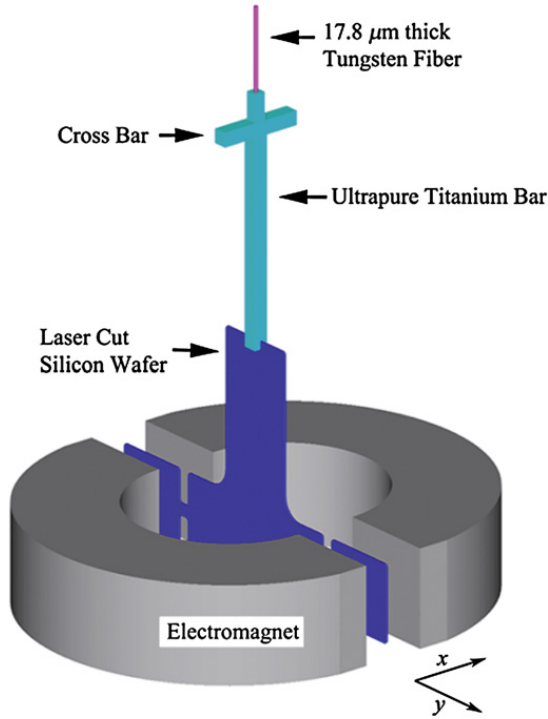
Fig. 11. The a scale diagram of the axion apparatus.

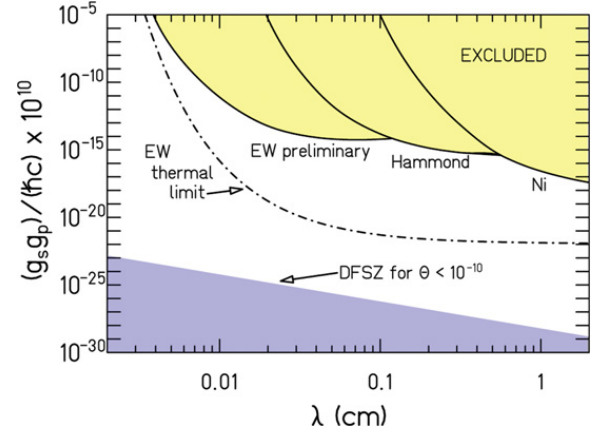**Fig. 11.** Dessin à l'échelle du dispositif pour la recherche de l'axion.

Fig. 12. The 2-σ exclusion plot on an axion mediated force.

Fig. 12. Zone d'exclusion à 2-σ pour une force induite par un axion.

In these models, the space–time coordinates x_μ do not commute, but instead satisfy $[\hat{x}_\mu, \hat{x}_\nu] = i\Theta_{\mu\nu}$, where $|\Theta|$ represents the smallest "patch" of area. The non-commutative geometry is equivalent to a pseudo-magnetic field that defines a preferred direction, $\eta_i = \epsilon^{ijk}\Theta_{jk}$. Our preferred-frame constraints imply that the minimum observable area is $|\Theta| \leqslant 4.9 \times 10^{-59}$ m^2, which corresponds to a length scale $\ell = 350 l_{GUT}$, where $l_{GUT} = {\sim}c/(10^{16}$ GeV).

A wide variety of extensions to the Standard Model predict the existence of light pseudo-scalar particles. Typically, these new particles correspond to a spontaneously broken symmetry and have a variety of names including familons, majorons, arions and axions. Pseudo-scalar particles are also predicted by string theories [174]. The axion is the most well developed pseudo-scalar and several experimental searches are actively underway. For simplicity, we refer to both axions and other pseudo-scalars as axion-like particles (ALPs).

Any ALP that couples to fundamental fermions with both scalar and pseudo-scalar vertices will mediate a parity and time violating (PTV) macroscopic force between polarized electrons and unpolarized nucleons [49] given by:

$$V_{PTV}(\hat{\sigma}, \vec{r}) = \frac{\hbar^2}{8\pi m_e}\left(\frac{g_s^N g_p^e}{\hbar c}\right)(\hat{\sigma} \cdot \hat{r})\left(\frac{1}{r\lambda_{ALP}} + \frac{1}{r^2}\right)e^{-r/\lambda_{ALP}} \tag{10}$$

where r is the electron–atom separation vector, $\lambda_{ALP} = m_{ALP}/\hbar c$ is the ALP Compton wavelength, $\hat{\sigma}$ and m_e are the spin unit-vector and mass of the polarized electron respectively, g_p^e is the ALP pseudo-scalar coupling constant to a polarized electron and g_s^N is the ALP scalar coupling constant to a nucleon. Although the spin-pendulum is very sensitive to a PTV force with $\lambda_{ALP} > 1$ m, for shorter ranges a dedicated experiment is necessary. λ_{ALP} between 2 cm and 20 μm is especially interesting because this range corresponds to the "axion-window" allowed by cosmological [175] and astrophysical limits [176].

The axion apparatus [51], consisted of two parts: a split toroidal electromagnet and a planar torsion pendulum suspended between the two magnet halves (see Fig. 11). The magnet halves were fixed to the apparatus; the pendulum was free to twist about the torsion fiber axis. The pendulum twist was observed by an autocollimator. The signal of a macroscopic PT violating force was a change in the equilibrium angle of the pendulum when the magnetic field was switched from the clockwise to counterclockwise orientation. Because the pendulum was suspended in a region with a strong magnetic field (3.59 kg), spurious signals associated with the finite magnetic susceptibility of the silicon dominated the data. Nevertheless, a constraint on an ALP mediated force was still obtained because an ALP force should strengthen when the pendulum is moved closer to either magnet half, whereas magnetic systematics depends only on the magnetic field. Thus, by measuring the ALP signal at different pendulum distances from the pole faces, we were able to constrain the PT violating force. Fig. 12 shows our 2-σ exclusion bounds.

After this part of the overview was written, new experimental results have been obtained and the final analysis of the experiment has been published in Ref. [51].
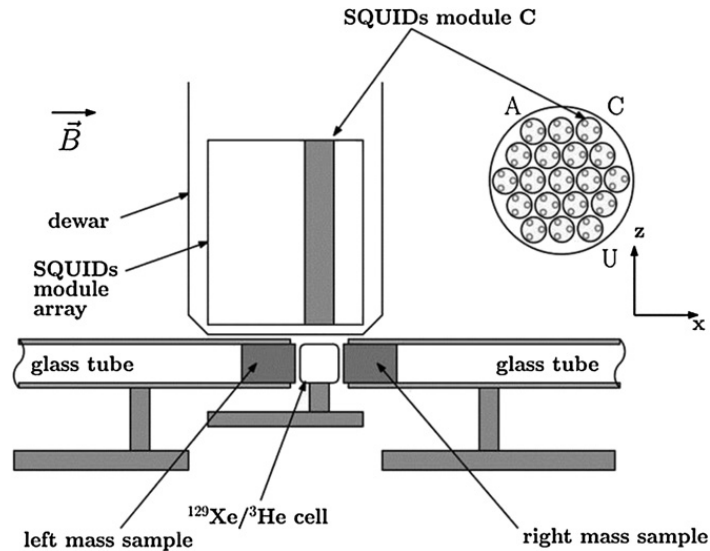
Fig. 13. A scheme of lay-out of the experimental setup.

Fig. 13. Schéma du principe du dispositif expérimental.

8. Constraints for spin-dependent short-range forces from storage of polarized ^{3}He (Alexander Petukhov)

New experimental constraints for spin-dependent short-range forces from storage of polarized ^{3}He are presented. A detailed description of the experimental method used, as well as justification for the constraints derived, is presented in Ref. [55].

9. Search for spin-dependent short-range interactions in ^{3}He/^{129}Xe clock comparison experiments (Yuri Sobolev, C. Gemmel, W. Heil, S. Karpuk, K. Lenz, K. Tullney, M. Burghoff, W. Kilian, S. Knappe-Gruneberg, W. Muller, A. Schnabel, F. Seifert, L. Trahms, U. Schmidt)

The existence of a new spin dependent short-range Yukawa force may be a signature of pseudo-scalar boson particles like the "invisible axion" which is of interest as a possible component of cold dark matter. Originally, the axion was invented by Peccei and Quinn [43] to solve the so-called "strong CP problem", i.e. presence of CP violating terms (θ-term) in the QCD Lagrangian that arise from the non-trivial QCD vacuum structure. Such axions were not found in early searches, ruling out "standard axions" which have been related to the electroweak scale of symmetry breaking in the original Peccei–Quinn model. However, in case of a much higher energy breaking scale the axion becomes a very light, very weakly coupled and very long-lived particle that is named "invisible axion" [175,176]. Such hypothetical particle can mediate interaction between fermions which in case of monopole–dipole coupling violates parity and time symmetries. The Yukawa-type potential of this monopole–dipole interaction with range λ can be presented in the following form [47]:

$$V_{SP}(r) = \frac{\hbar^2}{8\pi m} g_S g_P (\sigma \cdot \hat{r}) \left(\frac{1}{\lambda r} + \frac{1}{r^2} \right) e^{-r/\lambda} \tag{11}$$

where g_S and g_P are dimensionless scalar and pseudo-scalar constants for the axion–fermion vertices, $\hat{r}$ is the unit distance vector from the polarized nucleus to the unpolarized matter, λ is the range of the Yukawa force ($\lambda = \hbar/m_a c \approx 20$ cm/m_a (μeV), m_a – axion mass), m is mass of nucleon and σ is the spin of the polarized nuclei. The potential (1) effectively acts near the surface of a massive unpolarized sample ($r \leqslant \lambda$) as a pseudo-magnetic field and gives rise to a change in spin precession frequency $\Delta\nu_{SP}$ with $\Delta\nu_{SP} = V_\Sigma/h$. The potential V_Σ is obtained by integration of $V_{SP}(r)$ from Eq. (11) over the volume of the massive sample.

Our approach to search for non-magnetic spin-dependent interactions is to use a sensitive low-field co-magnetometer based on simultaneous detection of free spin precession of gaseous, nuclear polarized ^{3}He and ^{129}Xe samples both placed in same glass cell, thus occupying the same volume, with a SQUID as magnetic flux detector [177]. The gyromagnetic ratios of ^{3}He and ^{129}Xe differ by a factor ~2.75, whereas the coupling to new spin-dependent forces is expected to be very similar for both isotopes. Then the influence of ambient magnetic fields can be canceled in weighted precession frequencies difference $\Delta\nu = \nu_{He} - \gamma_{He}/\gamma_{Xe} \cdot \nu_{Xe}$ and it rests sensitive to the anomalous frequencies shifts coupled with new interactions with proportionality factor ~1.2 as it was calculated in [178]. The experiment was carried out inside the magnetically shielded room BMSR-2 at the Physikalisch-Technische Bundesanstalt Berlin (PTB). BMSR-2 has a passive shielding factor exceeding 10^8 above 6 Hz. A homogeneous holding magnetic field of about 400 nT was provided inside the shielded room by means one (B_x-coil) of two square coil pairs which were arranged perpendicular to each other whereas second (B_y-coil) was used to manipulate with spins of samples and their precession [177]. The experimental setup is shown in Fig. 13. For detection of

Table 2

Results for measured shifts of the weighted precession frequencies difference which can be sensitive to a new pseudo-scalar short-range interactions.

Measurement	v (nHz)	σ_{corr} (nHz)	σ_{stat} (nHz)
$v_{SP,left}$	46.6	11.1	1.4
$v_{SP,right}$	37.0	8.6	0.6
δv	4.8	7.0	0.5

the spin precession we used a low-T_c DC-SQUID vector magnetometer system designed for biomagnetic applications [179, 180]. To obtain signals of the precessing magnetic moments of the polarized gases (^{3}He, ^{129}Xe) we used a subset of SQUIDs which act as first order SQUID gradiometer. The pick-up coils of the gradiometer were oriented in the horizontal plane and the lower 3 coils were placed at a distance of 24 mm from the bottom plate of Dewar whereas the upper coil was at 14 cm higher. The lower pick-up coils of the SQUID modules are shown in Fig. 13 in the top-right corner. The system noise of the SQUIDs was about 2.3 fT/$\sqrt{\text{Hz}}$ in precession frequencies range. Most part of the environmental noise was from the effect of Dewar vibration relative to the B_x coil. However, the use of a SQUID gradiometer helps to suppress this effect down to level not higher than 2.5 fT/$\sqrt{\text{Hz}}$. Our cylindrical cell was made out of aluminosilicate glass (GE180) with a diameter of 60 mm and a length of 60 mm. The spin-relaxation time (longitudinal wall relaxation time T_1) of ^{3}He was measured to be $T_1 \approx 127$ h. The cell was filled outside the magnetic shielded room with a mixture of polarized ^{3}He and ^{129}Xe (≈ 2 mbar, ≈ 8 mbar) and N$_2$ (≈ 35 mbar) to suppress xenon relaxation due to the van der Waals molecular coupling. After transportation into the inner shield the cell was installed directly beneath the selected SQUIDs of the Dewar. Two cylindrical glass tubes with a length of 1 m and an inner diameter of 60 mm were placed on a separate support with their axis along the axis of the cylindrical ^{3}He/^{129}Xe sample cell. At their open ends towards the polarized sample cell a test mass (Pb-glass) was installed. This is sketched in Fig. 13. The tubes and with it the test mass could be moved horizontally from "close" position to "far away"-position. At the "close"-position we had a minimum distance of 3 mm between the Pb-glass samples and the polarized gases. The glass tubes were installed in such a way that it was possible to move them without opening the door of the magnetic shielded room, i.e., without interruption of the ^{3}He/^{129}Xe spin precession. Pb-glass cylinders (density 3.9 g/cm^3) of diameter 57 mm and length 81 mm were used, since non-conducting materials prevented us from additional noises sources. If axion–fermion interaction exists then it will cause a shift in the weighted precession frequencies difference $\pm v_{SP}$ where the sign depend on direction of the normal vector to the surface of the Pb-glass sample relative to the direction of the holding magnetic field. Therefore, to look for an effect with the right signature, the measurement procedure was as follows: first, we measured the precession signals where only left Pb-glass sample was installed with the first time interval (10 800 sec) measured at "close"-position and then we continue measurement during second time interval ($\sim$30 000 sec) when the Pb-glass sample was at "far away"-position. Second, we repeated the same procedure, now with right Pb-glass sample. To extract the precession frequencies we divided the data into sequential time intervals of ($\sim$1–3 sec) and for each time interval (j) we applied the fit: $A(t) = A_{\text{He}} \cdot \sin(\omega_{\text{He}} \cdot t) + B_{\text{He}} \cdot \cos(\omega_{\text{He}} \cdot t) + A_{\text{Xe}} \cdot \sin(\omega_{\text{Xe}} \cdot t) + B_{\text{Xe}} \cdot \cos(\omega_{\text{Xe}} \cdot t) + c_{lin} \cdot t + c$. Phases can be found as $\Phi_i^j = \arctan(A_i^j / B_i^j) + 2\pi \cdot n_i^j$ where n_i^j are the number of precession periods since the beginning of the measurement for $i = $ He, Xe. In order to cancel the influence of ambient magnetic fields we build the weighted phase difference of the co-located precessing spin samples: $\Delta\phi = \phi_{\text{He}} - \gamma_{\text{He}}/\gamma_{\text{Xe}} \cdot \phi_{\text{Xe}}$ with $\gamma_{\text{He(Xe)}}$ being the respective gyromagnetic ratios. It was found and discussed in detail in [177] the weighted phase difference has the following temporal dependence:

$$f(t) = \phi_0 + a_{lin} \cdot t + a_{\text{He}} \cdot e^{-t/T2,\text{He}} + a_{\text{Xe}} \cdot e^{-t/T2,\text{Xe}}$$

where $T2$, He(Xe) are the respective transverse relaxation times for ^{3}He and ^{129}Xe. In our analysis, we used a polynomial fit with sufficiently high order to describe $f(t)$ and the effect was sought as difference between the linear terms of the polynomial for measurements with mass sample ("close"-position) and without ("far away"-position):

$$v_{SP,left(right)} = 1/2\pi \, (a_{lin,with\,sample} - a_{lin,without\,sample})$$

Finally, we obtained the effect by combining the "left" and "right" Pb-glass measurements: $\delta v = 1/2 \, (v_{SP,left} - v_{SP,right})$. Results for $v_{SP,left(right)}$ and δv are given in Table 2. One can see that the "left" and "right" results in a frequency offset of the same sign and size. This is obviously a false effect since for a pseudo-scalar coupling the sign should change.

The reasons are induced magnetic field gradients (paramagnetism) across the cell by the Pb-glass sample in its "close"-position. With the weighted phase difference of the co-located sample spins, the Zeeman-term should drop out to first order. Taking into account the barometric formula the center of gravity of the ^{3}He and ^{129}Xe gas is shifted by 0.15 μm. This results in a field change of 0.3 fT at an induced field gradient of 20 pT/cm. With that one can explain the observed frequency offset. However, in the combination δv of the two measurements this effect drops out and we are left with a possible frequency shift, due to a pseudo-scalar short-range interaction. It is true, that only two measurements are not enough to check all the systematic and to finally obtain a statistically confirmed confidence level. But our result can be considered as a demonstration of the sensitivity one obtains by using co-located ^{3}He/^{129}Xe sample spins. In Table 2 we show correlated and uncorrelated errors obtained from the polynomial fit. Obviously the correlated error is much bigger than the uncorrelated one. This is understood from the fitting procedure of $f(t)$. The σ_{corr} errors are calculated as square
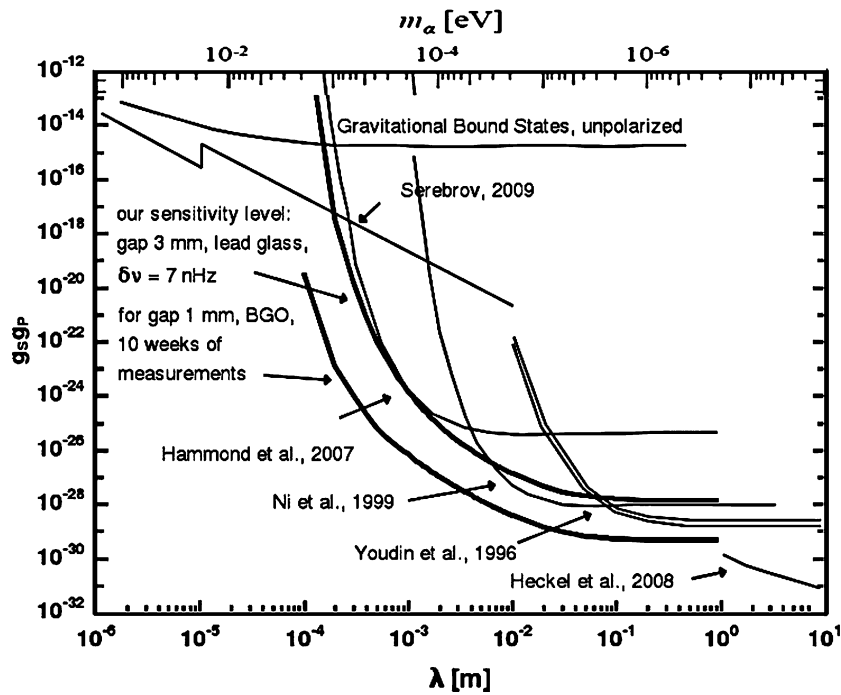
Fig. 14. Exclusion plot for a new spin-dependent force [163,52,51,50,185,56].
Fig. 14. Figure d'exclusion pour une nouvelle force dépendante du spin [163,52,51,50,185,56].

root of the diagonal elements of the covariance matrix of the polynomial least squares model with the proper statistical weights. This error for δv can be used to set our sensitivity level for the dimensionless product $g_S g_P$ in the exclusion plot shown in Fig. 14 (thick black curve). This result follows from $\bar{V}_\Sigma / h < \sigma_{corr}$, where $\bar{V}_\Sigma$ is sum of potentials (7) over the volume of the Pb-glass sample averaged over the ^{3}He/^{129}Xe cell volume. Also shown (second thick curve in Fig. 14) is the exclusion level which we can achieve for longer measurement periods (10 weeks) using as unpolarized matter BGO crystals (almost twice more dense) and furthermore using a much smaller minimum gap between the polarized (^{3}He/^{129}Xe) and unpolarized sample (BGO). The obtained statistical sensitivity level shown in Table 2 also demonstrates that further progress can be achieved by suppression of the correlated error. Ways to do that are discussed in the appendix of Ref. [177].

10. Constraints for short-range forces from neutron experiments (Konstantin Protasov)

The constraints obtained in Ref. [12] come from the analysis of quite old experimental data on neutron–nucleus and neutron–atom scattering. Two main approaches were used to obtain these limits.

First, at very low energies, neutron–nucleus scattering amplitude, in the first approximation, can be considered as constant independent on the transferred momentum, called the neutron–nucleus scattering length. However, this constant depends on nucleus and this dependence was studied experimentally and can be described within quite simple random square well model. An additional hypothetical interaction is directly proportional to the number of nucleons in nucleus A. This dependence is not seen in the experimental data and thus the data can be used to establish an upper limit for the strength of this hypothetical interaction. In the second approximation, an interaction between a neutron and an atom has an angular dependence following from the interaction between the distribution of charges in a neutron and charges of electrons and a nucleus. This interaction is proportional to the so-called electron–neutron scattering length. There are different ways to measure this scattering length and these independent measurements could be used to constraint any other additional interaction depending on the transferred momentum. The problem comes from the fact that the measurements of this scattering length done by different experimental groups contradict to each other. This discrepancy shows that the experimental errors are underestimated and should be increased. Nevertheless, even in this case, this approach allows establishing very competitive constraints on the hypothetical interaction.

11. Constraints for spin-dependent interactions from neutron-EDM experiments (Guillaume Pignol)

Constraints for spin-dependent interactions from could also be derived from neutron-EDM experiments using ultra-cold neutrons (see Fig. 3).

12. Neutron diffraction constraint on spin-dependent short-range interaction (Valery Fedorov, I.A. Kuznetsov, and V.V. Voronin)

Over the last years, a possibility to look for new hypothetic particles which results in a new short range Yukawa-type potential of fermion–fermion interaction is actively discussed. The spin-dependent short-range interactions may be induced by light, pseudo-scalar bosons such as the axion invented to solve the strong CP problem [49]. This interaction is usually parameterized as [49]:

$$V_{SP}(\mathbf{r}) = \frac{\hbar^2 g_S g_P}{8\pi m} \left(\frac{\mathbf{r}}{r} \cdot \sigma\right)\left(\frac{1}{r\lambda} + \frac{1}{r^2}\right) e^{-r/\lambda} \tag{12}$$

where g_S and g_P are dimensionless parameters of the scalar and pseudo-scalar coupling constants between the neutron and exchanged boson. $\lambda = \hbar/m_A c$ is typical parameter of the range of forces (Compton wavelength of axion). There are proposals to search this new type of interaction using gravitationally bound quantum states of a free neutron [58] and using a spin precession of the trapped ultra-cold neutrons in vicinity of bulk matter [181]. Both of these methods have a suitable sensitivity for the range of $\lambda > 10^{-3}$ cm, but their sensitivity is extremely decreased for the range $\lambda < 10^{-4}$ cm.

Here we consider a possibility to use neutron diffraction in the perfect non-centrosymmetric crystal to search a new type of short range interaction for the $10^{-10} < \lambda < 10^{-5}$ cm.

Neutron diffraction in a non-centrosymmetric crystal was widely discussed within the framework of the project to search for the neutron electric dipole moment (nEDM) by the diffraction method [182,183]. A series of experiments on neutron diffraction and optics was carried out at WWR-M reactor (PNPI, Gatchina) [184] and at ILL reactor [185] to study the polarization phenomena in the non-centrosymmetric quartz crystals.

Any crystal potential (nuclear, electric, new short range potential, ...) can be presented as sum of the potentials of different atoms placed into the crystal cell. For the periodic crystal structure it is convenient to present such potential as Fourier series over the reciprocal lattice vectors g

$$V(\mathbf{r}) = \sum_a V_a(\mathbf{r} - \mathbf{r}_a) = \sum_g V_g e^{i\mathbf{g}\mathbf{r}} = V_0 + \sum_g 2v_g \cos(\mathbf{g}\mathbf{r} + \phi_g) \tag{13}$$

where $V_a(\mathbf{r} - \mathbf{r}_a)$ is the potential of single atom, $\mathbf{r}_a$ is the atom position, $V_g = v_g \exp(i\phi_g)$, $g = 2\pi/d$, d is the inter-planar distance. Here we take into account $V_g = V_{-g}^*$, because we consider the real value potentials.

g-harmonics of potentials can be found from the equation

$$V_g = \int_{v=1} \mathrm{d}^3 r \, e^{-i\mathbf{g}\mathbf{r}} V(\mathbf{r}) \tag{14}$$

In the case of nuclear potential

$$V_g = -\frac{2\pi \hbar^2}{m V_c} F_g \tag{15}$$

here m is the neutron mass, V_c is volume of crystal unit cell, F_g is the structure amplitude

$$F_g = \sum_i e^{-W_{ig}} f_i(\mathbf{g}) e^{-i\mathbf{g}\mathbf{r}_i} \tag{16}$$

Here we sum over the atoms of unit cell, $f(\mathbf{g})$ is the scattering amplitude of i atom, W_{ig} is the Debye–Waller temperature factor.

For the case of a non-centrosymmetric crystal the different potentials can be shifted to each others, by the other words, the phases ϕ_g of different crystal potentials can be not equal. For the case of electric potential this shift results in a large electric field affected the neutron in non-centrosymmetric crystal [184–186]. Let's consider the monopole–dipole interaction (12). Direct calculation of g-harmonic of $V_{SP}(\mathbf{r})$ from (14) gives

$$\hat{V}_g^{SP} = -i F_g^{SP} e^{i\Phi_g^{SP}} \frac{\hbar^2 g_s g_p}{2m V_c} \frac{g\lambda^2}{1 + g^2\lambda^2} (\sigma \mathbf{n}_g) \tag{17}$$

where $\mathbf{n}_g \equiv g/g$, F_g^{SP} and Φ_g^{SP} are the amplitude and phase of structure factor f_g^{SP} of the crystallographic plane. f_g^{SP} is determined by the following sum

$$f_g^{SP} = \sum_i A_i \cdot e^{i\mathbf{g}\mathbf{r}_i} \tag{18}$$

here A_i and $\mathbf{r}_i$ is the mass and position of a corresponding atom in elementary cell.
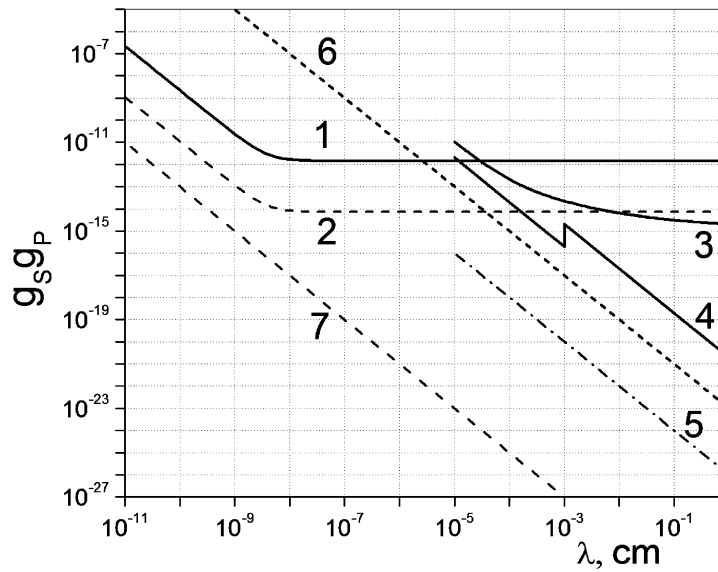
Fig. 15. Constraints on a value of coupling constants product $g_s g_p$. Curve (1) is the constraint from the crystal-diffraction nEDM experiment [185] (this work) and (2) is possible improvement of this method, (3) is gravitational level experiment [58], (4) is the UCN depolarization [61], (5) is proposal [181], (6) and (7) are the predictions of axion model with $\theta \sim 1$ and $\theta \sim 10^{-10}$ correspondingly [61,187].

Fig. 15. Contraintes sur le produit des constantes de couplages $g_s g_p$. La courbe (1) indique la contrainte à partir de l'expérience de crystal-diffraction nEDM [185] (cette étude) et (2) indique l'amélioration possible de cette méthode. La ligne (3) concerne l'expérience des niveaux gravitationnels, (4) la dépolarisation des UCNs [61], (5) est la proposition [181], (6) et (7) sont les prédictions du modèle axion avec $\theta \sim 1$ et $\theta \sim 10^{-10}$ respectivement [61,187].

Therefore, the monopole–dipole interaction affecting the neutron in the crystal will be

$$\hat{V}_{SP} = \langle \psi(\mathbf{r}) | V_{SP}(\mathbf{r}) | \psi(\mathbf{r}) \rangle = \frac{U_g^N}{\Delta_g} |\hat{V}_g^{SP}| \sin \Phi_g^{SP}$$

$$= \frac{U_g^N}{\Delta_g} F_g^{SP} \frac{\hbar^2 g_s g_p}{2m V_c} \frac{g\lambda^2}{1 + g^2\lambda^2} (\boldsymbol{\sigma} \mathbf{n}_g) \sin \Phi_g^{SP} \equiv V_{SP}(\boldsymbol{\sigma} \mathbf{n}_g) \tag{19}$$

here $k_g = k + g$, $E_k = \hbar^2 k^2/2m$, $E_{k_g} = \hbar^2 k_g^2/2m$, $V_g^N = \hbar^2 U_g^N/2m$, $\Delta_g = (k_g^2 - k^2)/2$ is the parameter of deviation from the exact Bragg condition.

We should note that for centrosymmetric crystal $\Phi_g^{SP} \equiv 0$ and in this case the mean potential affecting the neutron will be zero. One can see also from (19) that this "pseudomagnetic" potential is proportional to the parameter $\Delta_B \equiv U_g/\Delta_g$ determined by the deviation from the Bragg condition. That allows controlling the value and sign of the potential selecting the neutrons with slightly different energies from the Bragg one.

Interaction with such a potential will lead to the neutron spin rotation around the reciprocal lattice vector g by the angle

$$\varphi_{SP} = \frac{2 V_{SP}}{\hbar} \tau \tag{20}$$

where τ is the time of neutron travel through the crystal.

Let's consider [110] plane of non-centrosymmetric quartz crystal and $\Delta_B = 0.5$. For [110] plane $g = 2.56 \cdot 10^8$ cm^{-1}, $F_g^{SP} = 51$, $\sin(\Phi_g^{SP}) = 0.41$, $V_c = 113$ Å^3. The angle of spin rotation due to considered potential will be

$$\varphi_{SP} = 0.36 \cdot 10^{24} [\text{cm}^{-3}] \cdot \frac{g_s g_P}{g^2 + 1/\lambda^2} L \tag{21}$$

where L is the crystal length. For the cold neutron beam at high flux reactor the measurement accuracy $\sigma(\varphi_{SP}) \sim 2 \cdot 10^{-6}$ can be reached for 100 day of the statistics accumulation [186]. That allows giving the constraint for monopole–dipole interaction

$$g_S g_P < 10^{-31} [\text{cm}^2] \cdot (g^2 + 1/\lambda^2) \tag{22}$$

for the $L = 50$ cm.

Recently the test experiment for the search for neutron EDM by crystal-diffraction method was carried out [185]. This result already allows to give the direct constraint on a value of $g_s g_P$ better than any other method for the $\lambda < 10^{-5}$ cm, see Fig. 15, curve (1).

The comparison of different constraints on $g_S g_P$ is shown in Fig. 15.

One should note that both neutron EDM interaction with crystal electric field and the spin-dependent short-range interaction lead to a neutron spin rotation about reciprocal lattice vector **g**. Therefore, the considered short-range interaction can give a false effect for the neutron EDM experiment and vice versa. However, these two interactions will be different for different crystallographic planes, so in the case of nonzero effect they can be separated using different planes for measurement.

We can conclude from the above consideration that crystal-diffraction experiment can give the direct constraint on amplitude of T-odd monopole–dipole interaction of neutron with the matter. It is shown that the product of scalar to pseudo-scalar coupling constant $g_s g_p < 10^{-12}$ for the $10^{-8} < \lambda < 10^{-5}$ cm. This value can be improved on about 10^3 times for the full scale setup for the neutron EDM search by crystal-diffraction method, which is under construction now.

13. Conclusion

We presented recent advances in experiments constraining spin-dependent and spin-independent extra short-range forces. Over a few recent years, large progress has been achieved using most of the experimental techniques presented here. In particular, the experimental constraints have been improved, in respective characteristic energy ranges, in measurements of gravity at short distances, in measurements of forces on top of Casimir forces, in precision atomic and neutron experiments. Most of these results are presented at our GRANIT-2010 workshop for the first time. They are summarized in Figs. 1 and 3. Even stronger improvements are expected in near future.

References

[1] I. Antoniadis, Phys. Lett. B 246 (1990) 377.
[2] J.D. Lykken, Phys. Rev. D 54 (1996) R3693.
[3] N. Arkani-Hamed, et al., Phys. Lett. B 429 (1998) 263.
[4] I. Antoniadis, et al., Phys. Lett. B 436 (1998) 257.
[5] V.A. Rubakov, et al., Phys. Lett. B 125 (136) (1983) 139.
[6] M. Visser, Phys. Lett. B 159 (1985) 22.
[7] A. Frank, et al., Phys. Lett. B 582 (2004) 15.
[8] D.L. Kapner, et al., Phys. Rev. Lett. 98 (2007) 021101.
[9] A.A. Geraci, et al., Phys. Rev. D 78 (2008) 022002.
[10] M. Bordag, et al., Phys. Rep. 353 (2001) 1.
[11] R.S. Decca, et al., Phys. Rev. Lett. 94 (2005) 240401.
[12] V.V. Nesvizhevsky, et al., Phys. Rev. D 77 (2008) 034020.
[13] H. Abele, et al., Lect. Notes Phys. 631 (2003) 355.
[14] V.V. Nesvizhevsky, K.V. Protasov, Class. Quant. Grav. 21 (2004) 4557.
[15] O. Zimmer, N. Kaiser, Class. Quant. Grav. 23 (2006) 6077.
[16] V.V. Nesvizhevsky, K.V. Protasov, Class. Quant. Grav. 23 (2006) 6081.
[17] A. Westphal, et al., arXiv:hep-ph/0703108.
[18] V.V. Nesvizhevsky, et al., Nature 415 (2002) 297.
[19] V.V. Nesvizhevsky, et al., Phys. Rev. D 67 (2003) 102002.
[20] V.V. Nesvizhevsky, et al., Europ. Phys. J. C 40 (2005) 479.
[21] S. Baessler, M. Beau, et al., C. R. Physique 12 (2011) 707, doi:10.1016/j.crhy.2011.04.010 (in this issue).
[22] S. Baessler, A.M. Gagarski, et al., C. R. Physique 12 (2011) 729, doi:10.1016/j.crhy.2011.04.014 (in this issue).
[23] T. Sanuki, et al., Nucl. Instrum. Methods A 600 (2009) 657.
[24] M. Kreuz, et al., Nucl. Instrum. Methods A 611 (2009) 326.
[25] T. Jenke, et al., Nucl. Instrum. Methods A 611 (2009) 318.
[26] G. Pignol, PhD thesis UJF, Grenoble, 2009.
[27] V.V. Nesvizhevsky, et al., Phys. Rev. A 78 (2008) 033616.
[28] V.V. Nesvizhevsky, et al., Nature Phys. 6 (2010) 114.
[29] V.V. Nesvizhevsky, et al., New J. Phys. 12 (2010) 113050.
[30] V.V. Nesvizhevsky, A.Yu. Voronin, C. R. Physique 12 (2011) 791, doi:10.1016/j.crhy.2011.07.001 (in this issue).
[31] H. Leeb, J. Schmiedmayer, Phys. Rev. Lett. 68 (1992) 1472.
[32] Yu.N. Pokotilovsky, Phys. At. Nucl. 69 (2006) 924.
[33] V. Gudkov, et al., Phys. Rev. C 83 (2011) 025501.
[34] Y. Kamyshkov, et al., Phys. Rev. D 78 (2008) 114029.
[35] R.S. Decca, et al., Europ. Phys. J. C 51 (2007) 963.
[36] U. Mohideen, et al., Phys. Lett. A 132 (1988) 313.
[37] E. Fischbach, et al., Phys. Rev. Lett. 94 (2005) 240401.
[38] S.K. Lamoreaux, et al., Phys. Rev. Lett. 78 (1997) 5.
[39] V.M. Mostepanenko, M. Novello, Phys. Rev. D 63 (2001) 115003.
[40] T. Ederth, Phys. Rev. A 62 (2000) 062104.
[41] J. Long, et al., Nucl. Phys. B 539 (1999) 23.
[42] S.K. Lamoreaux, Phys. Rev. A 82 (2010) 024102.
[43] R. Horvat, et al., Phys. Lett. B 699 (2011) 21.
[44] R.D. Peccei, et al., Phys. Rev. Lett. 38 (1977) 1440.
[45] R.D. Peccei, et al., Phys. Rev. D 16 (1977) 1791.

[46] S. Weinberg, Phys. Rev. Lett. 40 (1978) 223.
[47] F. Wilczek, Phys. Rev. Lett. 40 (1978) 279.
[48] M. Kuster, et al., Lect. Not. Phys. 741 (2008) 1.
[49] J.E. Moody, F. Wilczek, Phys. Rev. D 30 (1984) 130.
[50] E. Adelberger, et al., Prog. Part. Nucl. Phys. 62 (2009) 102.
[51] S.A. Hoedl, et al., Phys. Rev. Lett. 106 (2011) 041801.
[52] G.D. Hammond, et al., Phys. Rev. Lett. 98 (2007) 081101.
[53] W.-T. Ni, et al., Phys. Rev. Lett. 82 (1999) 2440.
[54] A.N. Youdin, et al., Phys. Rev. Lett. 77 (1996) 2171.
[55] A.K. Petukhov, et al., Phys. Rev. Lett. 105 (2010) 170401.
[56] C.B. Fu, et al., Phys. Rev. D 83 (2011) 031504.
[57] A.K. Petoukhov, et al., arXiv:1103.1770.
[58] S. Baessler, et al., Phys. Rev. D 75 (2007) 075006.
[59] A.P. Serebrov, et al., JETP Lett. 91 (2010) 6.
[60] O. Zimmer, et al., Phys. Lett. B 685 (2010) 38.
[61] A.P. Serebrov, et al., Phys. Lett. B 680 (2009) 423.
[62] V.K. Ignatovich, et al., Europ. Phys. J. C 64 (2009) 19.
[63] H. Abele, et al., Phys. Rev. D 81 (2010) 065019.
[64] O. Zimmer, Phys. Lett. B 685 (2010) 38.
[65] J.C. Long, J.C. Price, C. R. Physique 4 (2003) 337.
[66] R.S. Decca, et al., Europ. Phys. J. C 51 (2007) 953.
[67] S.J. Smullin, et al., Phys. Rev. D 72 (2005) 122001; Erratum: Phys. Rev. D 72 (2005) 129901.
[68] I. Antoniadis, C. Bachas, Phys. Lett. B 450 (1999) 83.
[69] N. Arkani-Hamed, et al., hep-th/9908146.
[70] I. Antoniadis, et al., Nucl. Phys. B 662 (2003) 40.
[71] I. Antoniadis, et al., Nucl. Phys. B 516 (1998) 70.
[72] S. Ferrara, et al., Nucl. Phys. B 429 (1994) 589.
[73] E.G. Adelberger, et al., Phys. Rev. Lett. 98 (2007) 131104.
[74] T.R. Taylor, G. Veneziano, Phys. Lett. B 213 (1988) 450.
[75] I. Antoniadis, et al., Nucl. Phys. B 637 (2002) 92.
[76] L. Randall, R. Sundrum, Phys. Rev. Lett. 83 (1999) 3370.
[77] H.B.G. Casimir, Proc. K. Ned. Akad. Wet. 51 (1948) 793.
[78] P.W. Milonni, The Quantum Vacuum, Academic, 1994.
[79] S.K. Lamoreaux, Resource Lett. Am. J. Phys. 67 (1999) 850.
[80] R.S. Decca, et al., Ann. Phys. 318 (2005) 37.
[81] A. Lambrecht, et al., New J. Phys. 8 (2006) 243.
[82] M.-T. Jaekel, S. Reynaud, in: Proc. Orleans School on Mass, arXiv:0812.3936, 2009.
[83] M.-T. Jaekel, S. Reynaud, Rep. Progr. Phys. 60 (1997) 863.
[84] A. Lambrecht, J. Opt. B 7 (2005) 3.
[85] R. Ballian, B. Duplantier, Ann. Phys. NY 104 (1977) 300.
[86] R. Balian, B. Duplantier, Ann. Phys. NY 112 (1978) 165.
[87] E. Fischbach, C. Talmadge, The Search for Non-Newtonian Gravity, AIP Press/Springer-Verlag, 1998.
[88] E.G. Adelberger, et al., Ann. Rev. Nucl. Part. Sci. 53 (2003) 77.
[89] R. Onofrio, New J. Phys. 8 (2006) 237.
[90] S. Lepoutre, et al., Europ. Phys. Lett. 88 (2009) 20002.
[91] A. Lambrecht, S. Reynaud, Europ. Phys. J. D 8 (2000) 309.
[92] J. Schwinger, et al., Ann. Phys. 115 (1978) 1.
[93] C. Genet, et al., Phys. Rev. A 62 (2000) 012110.
[94] M. Bostrom, B.E. Sernelius, Phys. Rev. Lett. 84 (2000) 4757.
[95] I. Brevik, et al., New J. Phys. 8 (2006) 236.
[96] G.-L. Ingold, et al., Phys. Rev. E 80 (2009) 041113.
[97] R. Decca, et al., Phys. Rev. D 75 (2007) 077101.
[98] B. Jancovici, L. Samaj, Europ. Lett. 72 (2005) 35.
[99] P.R. Buenzli, Ph.A. Martin, Europ. Lett. 72 (2005) 42.
[100] G. Bimonte, Phys. Rev. A 79 (2009) 042107.
[101] A.O. Sushkov, et al., Nature Phys. 7 (2011) 230.
[102] K. Milton, Nature Phys. 7 (2011) 190.
[103] B.V. Deriagin, et al., Quart. Rev. 10 (1968) 295.
[104] E.M. Lifshitz, Sov. Phys. JETP 2 (1956) 73.
[105] I.E. Dzyaloshinskii, et al., Sov. Phys. Uspekhi 4 (1961) 153.
[106] R.L. Jaffe, A. Scardicchio, Phys. Rev. Lett. 92 (2004) 070402.
[107] S. Reynaud, et al., J. Phys. A 41 (2008) 164004.
[108] T. Emig, R.L. Jaffe, J. Phys. A 41 (2008) 164001.
[109] M. Bordag, V. Nikolaev, J. Phys. A 41 (2008) 164002.
[110] K. Klingmuller, H. Gies, J. Phys. A 41 (2008) 164042.
[111] A. Canaguier-Durand, et al., Phys. Rev. Lett. 102 (2009) 230404.
[112] D.E. Krause, et al., Phys. Rev. Lett. 98 (2007) 050403.
[113] F. Chen, et al., Phys. Rev. Lett. 88 (2002) 101801.
[114] F. Chen, et al., Phys. Rev. A 66 (2002) 032113.
[115] R. Buscher, T. Emig, Phys. Rev. Lett. 94 (2005) 133901.
[116] P.A. Maia Neto, et al., Europ. Lett. 69 (2005) 924.
[117] P.A. Maia Neto, et al., Phys. Rev. A 72 (2005) 012115.
[118] B.R. Bodrigues, et al., Phys. Rev. Lett. 96 (2006) 100402.
[119] R.B. Rodrigues, et al., Phys. Rev. Lett. 98 (2007) 068902.

[120] R.B. Rodrigues, et al., Phys. Rev. A 75 (2007) 062108.
[121] H.B. Chan, et al., Phys. Rev. Lett. 101 (2008) 030401.
[122] H.C. Chiu, et al., Phys. Rev. B 80 (2009) 121402.
[123] A. Lambrecht, V.N. Marachevsky, Phys. Rev. Lett. 101 (2008) 160403.
[124] A. Lambrecht, Nature 454 (2008) 836.
[125] M.T. Jaekel, S. Reynaud, J. Phys. I 1 (1991) 1395.
[126] C. Genet, et al., Phys. Rev. A 67 (2003) 043811.
[127] T. Emig, Stat. Mech.: Theory Exp. P04007 (2008).
[128] O. Kenneth, I. Klich, Phys. Rev. B 78 (2008) 014103.
[129] K.A. Milton, J. Wagner, J. Phys. A 41 (2008) 155402.
[130] R.B. Rodrigues, et al., Europhys. Lett. 76 (2006) 822.
[131] D.A.R. Dalvit, et al., Phys. Rev. Lett. 100 (2008) 040405.
[132] R. Messina, et al., Phys. Rev. A 80 (2009) 022119.
[133] H. Gies, A. Weber, arXiv:0912.0125, 2009.
[134] M. Bordag, I. Pirozhenko, arXiv:0912.4047, 2009.
[135] A. Canaguier-Durand, et al., Phys. Rev. Lett. 104 (2010) 040403.
[136] M. Bordag, V. Nikolaev, Phys. Rev. D 81 (2010) 065011.
[137] A. Lambrecht, et al., Lect. Notes Phys., 2010, in press, arXiv:1006.2959.
[138] A.D. Cronin, et al., Rev. Mod. Phys. 81 (2009) 1051.
[139] C.R. Ekstrom, et al., Phys. Rev. A 51 (1995) 3883.
[140] A. Miffre, et al., Phys. Rev. A 73 (2006) 011603.
[141] B. Deissler, et al., Phys. Rev. A 77 (2008) 031604.
[142] J. Schmiedmayer, et al., Phys. Rev. Lett. 74 (1995) 1043.
[143] T.D. Roberts, et al., Phys. Rev. Lett. 89 (2002) 200406.
[144] M. Jacquey, et al., Phys. Rev. Lett. 98 (2007) 240405.
[145] http://www.cfa.harvard.edu/~babb/casimir-bib.html.
[146] R.E. Grisenti, et al., Phys. Rev. Lett. 83 (1999) 1755.
[147] M. Boustimi, et al., Europ. Phys. J. D 17 (2001) 141.
[148] B. Brezger, et al., Phys. Rev. Lett. 88 (2002) 100404.
[149] A. Landragin, et al., Phys. Rev. Lett. 77 (1996) 1464.
[150] J.D. Perreault, A.D. Cronin, Phys. Rev. Lett. 95 (2005) 133201.
[151] A. Miffre, et al., Europ. Phys. J. D 33 (2005) 99.
[152] S. Lepoutre, et al., Europ. Phys. J. D, submitted for publication.
[153] V.P.A. Lonij, Phys. Rev. A 80 (2009) 062904.
[154] J. Israelachvili, D. Tabor, Proc. R. Soc. Lond. A 331 (1972) 19.
[155] M. Bordag, et al., Phys. Lett. A 60 (1994) 35.
[156] H. Leeb, J. Schmiedmayer, Phys. Rev. Lett. 68 (1992) 1472.
[157] H. Abele, Progr. Part. Nucl. Phys. 60 (2008) 1.
[158] A. Hibbert, et al., J. Phys. B 20 (1987) L349.
[159] O. Bertolami, F.M. Nunes, Class. Quant. Grav. 20 (2003) L61.
[160] O. Bertolami, et al., Phys. Rev. D 72 (2005) 025010.
[161] O. Bertolami, J.G. Rosa, Phys. Lett. B 633 (2006) 111.
[162] O. Bertolami, et al., Mod. Phys. Lett. A 21 (2006) 795.
[163] C. Bastos, O. Bertolami, Phys. Lett. A 372 (2008) 5556.
[164] S. Baessler, et al., Nucl. Instrum. Methods A 611 (2009) 149.
[165] B.R. Heckel, et al., Phys. Rev. D 78 (2008) 092006.
[166] R. Sundrum, Phys. Rev. D 69 (2004) 044014.
[167] G. Dvali, et al., arXiv:hep-ph/9910207, 1999.
[168] E.G. Adelberger, et al., Phys. Rev. Lett. 98 (2007) 131104.
[169] A. Dupays, et al., Phys. Rev. Lett. 98 (2007) 131802.
[170] E. Zavattini, et al., Phys. Rev. Lett. 96 (2006) 110406.
[171] E. Zavattini, et al., Phys. Rev. D 77 (2007) 032006.
[172] S.M. Carroll, et al., Phys. Rev. Lett. 87 (2001) 141601.
[173] I. Hinchliffe, et al., Int. J. Mod. Phys. A 19 (2004) 179.
[174] P. Svrcek, E. Witten, J. High Energy Phys. 6 (2006) 51.
[175] S.J. Asztalos, et al., Ann. Rev. Nucl. Part. Sci. 56 (2006) 293.
[176] G.G. Raffelt, Ann. Rev. Nucl. Part. Sci. 49 (1999) 163.
[177] J.E. Kim, Phys. Rev. Lett. 43 (1979) 103.
[178] M. Shifman, et al., Nucl. Phys. B 166 (1980) 493.
[179] C. Gemmel, et al., Europ. Phys. J. D 57 (2010) 303.
[180] G. Glenday, et al., Phys. Rev. Lett. 101 (2008) 261801.
[181] O. Zimmer, Phys. Lett. B 685 (2010) 38.
[182] V.V. Fedorov, et al., J. Phys. G 18 (1992) 1133.
[183] V.V. Voronin, V.V. Fedorov, in: Frontiers in Condensed Matter Physics Research, Nova Science, New York, 2006, pp. 13–39.
[184] V.V. Fedorov, et al., Nucl. Instrum. Methods B 252 (2006) 131.
[185] V.V. Fedorov, et al., Nucl. Instrum. Methods A 611 (2009) 124.
[186] V.L. Alekseev, et al., Nucl. Instrum. Methods A 284 (1989) 181.
[187] G. Raffelt, Lect. Notes Phys. 741 (2008) 51.